Geol. Mag. **152** (2), 2015, pp. 316–340. © Cambridge University Press 2014
doi:10.1017/S0016756814000399

Reaction textures and metamorphic evolution of sapphirine–spinel-bearing and associated granulites from Diguva Sonaba, Eastern Ghats Mobile Belt, India

DIVYA PRAKASH*†, DEEPAK*, PRAVEEN CHANDRA SINGH*, CHANDRA KANT SINGH*, SUPARNA TEWARI*, MAKOTO ARIMA‡ & HARTWIG E. FRIMMEL§¶

*Centre of Advanced Study in Geology, Banaras Hindu University, Varanasi – 221 005, India
‡Geological Institute, Yokohama National University, 79-7 Tokiwadai, Hodogaya-ku, Yokohama 240-8501, Japan
§Institute of Geography and Geology, University of Würzburg, Am Hubland, D-97074 Würzburg, Germany
¶Department of Geological Sciences, University of Cape Town, Rondebosch 7701, South Africa

(*Received* 5 December 2013; *accepted* 1 July 2014; *first published online* 14 August 2014)

Abstract – The Diguva Sonaba area (Vishakhapatnam district, Andhra Pradesh, South India) represents part of the granulite-facies terrain of the Eastern Ghats Mobile Belt. The Precambrian metamorphic rocks of the area predominantly consist of mafic granulite (± garnet), khondalite, leptynite (± garnet, biotite), charnockite, enderbite, calc-granulite, migmatic gneisses and sapphirine–spinel-bearing granulite. The latter rock type occurs as lenticular bodies in khondalite, leptynite and calc-granulite. Textural relations, such as corroded inclusions of biotite within garnet and orthopyroxene, resorbed hornblende within pyroxenes, and coarse-grained laths of sillimanite, presumably pseudomorphs after kyanite, provide evidence of either an earlier episode of upper-amphibolite-facies metamorphism or they represent relics of the prograde path that led to granulite-facies metamorphism. In the sapphirine–spinel-bearing granulite, osumilite was stable in addition to sapphirine, spinel and quartz during the thermal peak of granulite-facies metamorphism but the assemblage was later replaced by Crd–Opx–Qtz–Kfs-symplectite and a variety of reaction coronas during retrograde overprint. Variable amounts of biotite or biotite + quartz symplectite replaced orthopyroxene, cordierite and Opx–Crd–Kfs–Qtz-symplectite at an even later retrograde stage. Peak metamorphic conditions of *c*. 1000 °C and *c*. 12 kbar were computed by isopleths of X_{Mg} in garnet and X_{Al} in orthopyroxene. The sequence of reactions as deduced from the corona and symplectite assemblages, together with petrogenetic grid and pseudosection modelling, records a clockwise *P–T* evolution. The *P–T* path is characteristically *T*-convex suggesting an isothermal decompression path and reflects rapid uplift followed by cooling of a tectonically thickened crust.

Keywords: sapphirine–spinel-bearing granulite, corona and symplectite textures, phase equilibria modelling, high-pressure – ultrahigh-temperature metamorphism, Eastern Ghats Mobile Belt, India.

1. Introduction

Dispersed mobile belts provide records of ever-changing continent configurations, especially the assembly and break-up of large continental masses throughout Earth's history (Condie, 2005). Ultrahigh-temperature (UHT) metamorphism that followed an isothermal decompression (ITD) path, as evident in some granulite terrains, is possibly a consequence of the existence of particularly large continents (Yoshida *et al.* 2003) and may thus hold clues for the reconstruction of former supercontinents. Such UHT–ITD metamorphism is preserved at several widely dispersed localities in the Indo-Antarctic region, with the Eastern Ghats Mobile Belt (EGMB) on the Indian subcontinent occupying a key position in the reconstruction of Meso- to Neoproterozoic continent configuration. Several occurrences of UHT-diagnostic metamorphic mineral assemblages in the EGMB have attracted petrologists to studying the area over the last decade (Dasgupta & Sengupta, 2003; Lal, 2003; Dasgupta, Raith & Sarkar, 2008; Mukhopadhyay & Basak, 2009; Dasgupta, Bose & Das, 2013). One of the diagnostic features of UHT metamorphism is the stable coexistence of sapphirine + quartz, which has been reported from a few localities in the EGMB (Lal, Ackermand & Upadhyay, 1987; Kamineni & Rao, 1988; Dasgupta *et al.* 1995; Bose *et al.* 2000; Dharma Rao, Santosh & Chmielowski, 2012). Apart from the assemblage sapphirine + spinel + quartz, that of highly aluminous orthopyroxene + sillimanite + quartz as well as the occurrence of osumilite are further indications of UHT metamorphism and have been noted in the EGMB (Lal, Ackermand & Upadhyay, 1987; Dasgupta *et al.* 1994; Bhattacharya & Kar, 2002).

In particular, sapphirine-bearing granulites have become the focus of numerous petrological studies in that area (Lal, Ackermand & Upadhyay, 1987; Kamineni &

†Author for correspondence: dprakashbhu@gmail.com

Rao, 1988; Sengupta *et al.* 1990, 1991, 1997*a*,*b*, 1999; Dasgupta *et al.* 1994, 1995; Shaw & Arima, 1996; Mohan, Tripathi & Motoyashi, 1997; Mukhopadhyay & Bhattacharya, 1997; Pal & Bose, 1997; Shaw & Arima, 1998; Bose *et al.* 2000, 2006; Gupta *et al.* 2000; Rickers, Mezger & Raith, 2001; Bhattacharya & Kar, 2002; Bhattacharya *et al.* 2003; Sarkar *et al.* 2003; Bose & Das, 2007; Das *et al.* 2011; Dharma Rao & Chmielowski, 2011; Korhonen *et al.* 2011; Dharma Rao, Santosh & Chmielowski, 2012). In addition, petrological studies on calc-silicate granulite (Dasgupta *et al.* 1993; Bhowmik *et al.* 1995) as well as mafic and orthopyroxene-bearing quartzo-feldspathic granulite (Dasgupta *et al.* 1991, 1993; Sengupta *et al.* 1996; Mohan, Singh & Sachan, 2003) have been carried out.

We discovered a hitherto unknown locality of sapphirine–spinel granulite that contains sapphirine + quartz in an area around Diguva Sonoba in the southwestern part of the EGMB (Fig. 1). In this paper we present new petrographic and mineral chemical data, based on which we provide new constraints on the metamorphic evolution of these UHT granulites as derived from well-constrained micro-structural relations, mineral assemblages and forward modelling (isochemical pseudosection). Our new results, in comparison with those from other localities of the EGMB, make it possible to re-evaluate the regional tectonothermal evolution of the EGMB.

2. Regional geology of the Eastern Ghats Mobile Belt

On the basis of dominant lithological assemblages, Ramakrishnan, Nanda & Augustine (1998) divided the EGMB into four broadly longitudinal zones (Fig. 1), which, from northwest to southeast, are: (i) the Western Charnockite Zone (WCZ), which consists of enderbite, mafic granulites and charnockite with enclaves of mafic–ultramafic rocks and minor amounts of metapelites; (ii) the Western Khondalite Zone (WKZ), which is dominated by khondalite, quartzite, calc-silicate rocks and sapphirine–spinel granulite; (iii) the Central Migmatite Zone (CMZ), which consists of migmatite gneisses and leptynites; and (iv) the Eastern Khondalite Zone (EKZ), which is lithologically similar to the WKZ. The metamorphic rocks of the EGMB display a gradual increase in metamorphic grade from the southwest to the northeast.

The ages of both the protoliths and metamorphic events in the EGMB remain poorly constrained. Whole-rock Rb–Sr (3100 ± 20 Ma in khondalite from Puri, Vinogradov *et al.* 1964; 2600 ± 63 Ma in charnockite, Paul *et al.* 1990), Sm–Nd (2900 ± 36 Ma in charnockites and mafic granulites, Paul *et al.* 1990) and inherited U–Pb zircon ages of 2580–2600 Ma (Vinogradov *et al.* 1964) point to an Archaean crustal component in the protoliths of the EGMB metamorphites.

Based on field relationships and petrography, three major deformational and metamorphic events can be distinguished. During an earlier granulite-facies metamorphism (M1), the supracrustal rocks were deformed under UHT conditions as evidenced by sapphirine–spinel–quartz-bearing parageneses found in various domains within the EGMB. Later, the EGMB was intruded by voluminous enderbitic charnockites that subsequently underwent deformation again under granulite-facies conditions (M2). This M2 event is widely recognized throughout the EGMB. Vast granite and anorthosite bodies that were emplaced post-M2 show evidence of further, retrograde metamorphic overprint (M3).

The absolute ages of the various metamorphic events remain enigmatic. Mezger & Cosca (1999) distinguished between two segments in the EGMB, separated by the Godavari Rift. The northern segment is dominated by age data around 1.0 to 0.5 Ga and Nd model ages of 3.9 to 3.2 Ga, whereas the southern segment is distinguished by a major thermal event around 1.6 Ga and Nd model ages between 2.3 and 2.8 Ga (Rickers, Mezger & Raith, 2001).

The age of the earlier UHT metamorphism (M1) preserved locally in Mg–Al-rich granulites remains open to debate. Both pre-Grenvillian and syn-Grenvillian ages have been suggested (Mezger & Cosca, 1999). Possible pre-Grenvillian ages are 1630 Ma (Upadhyay, Gerdes & Raith, 2009) and *c*. 1760 Ma (Bose *et al.* 2011), the age of mafic magmatism (Sengupta *et al.* 1999). Most recent U–Pb age determinations on *in situ* zircon and monazite grains indicate UHT metamorphic conditions having lasted for at least 50 Ma, possibly as long as 200 Ma, from *c*. 1130 to 930 Ma (Korhonen *et al.* 2013), supporting previous age data of 1030 to 990 Ma from Bose *et al.* (2011).

In Pan-African times, the EGMB experienced a further major thermal overprint at amphibolite-facies conditions. This is indicated by a U–Th–Pb age of 573 ± 2 Ma obtained on syntectonic monazite in garnet–sillimanite gneiss (Upadhyay *et al.* 2006) and emplacement of nepheline syenite, pegmatite and megacrystic granite at around the same time (Paul *et al.* 1990; Aftalion *et al.* 2000; Upadhyay *et al.* 2006). No evidence of Pan-African granulite-facies metamorphism exists, however, in the EGMB.

3. Geological setting of the study area

Diguva Sonaba is situated at about 120 km northwest of the Vishakhapatnam district, Andhra Pradesh, within the granulite terrain of the EGMB. The study area (longitude 82° 50′ E to 82° 58′ 25″ E and latitude 18° 10′ N to 18° 13′ 29″ N) comprises a variety of granulitic rocks, mainly charnockites, mafic granulites, leptynite, khondalite, sapphirine–spinel granulite, calc-granulite and migmatitic gneisses (Fig. 1). All of these rocks were subjected to polyphase deformation and metamorphism. Garnet-bearing charnockite is coarse to medium grained and dark grey in colour (Fig. 2a). Mafic granulite is coarse to medium grained and dark (Fig. 2b). Leptynite is characterized by a massive fabric due to a predominance of K-feldspar and quartz (Fig. 2c). Veins of perthite and quartz are present.

https://doi.org/10.1017/S0016756814000399 Published online by Cambridge University Press

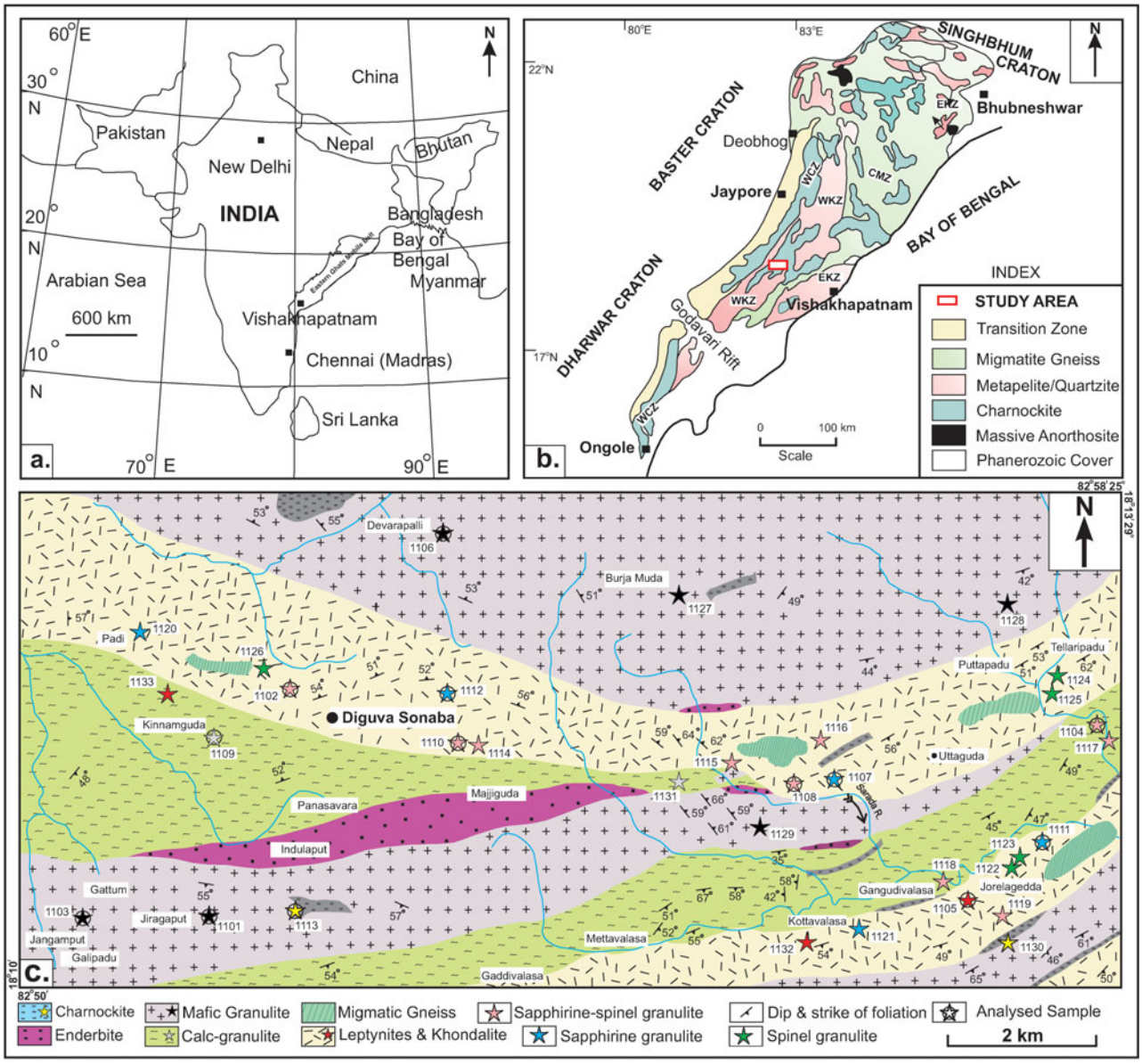

Figure 1. (Colour online) (a) Reference map of India showing the position of the Eastern Ghats Mobile Belt. (b) Lithological map of the Eastern Ghats Mobile Belt (after Ramakrishnan, Nanda & Augustine, 1998). Abbreviations: WCZ – Western Charnockite Zone; WKZ – Western Khondalite Zone; CMZ – Central Migmatite Zone; EKZ – Eastern Khondalite Zone. (c) Geological map of the area around Diguva Sonaba.

Evenly distributed small garnet grains are common to many of these rocks (Fig. 2c). Garnet porphyroblasts of up to 4 × 3 cm in size (Fig. 2d) are present in the leptynite. Pale to pinkish coloured khondalite is the dominant rock type in the study area (Fig. 2e). The oldest magmatic rocks in the area are the protoliths of mafic granulite that occur intercalated with khondalite and charnockite. The migmatites show layers of parallel leucosomes with thicker melanosomes (Fig. 2f), suggesting formation by grain-scale distribution of melt, because grain-scale flow is probably ineffective at transferring melt over large distances (Rutter, 1997). Sapphirine–spinel-bearing granulite is coarse to medium grained and dark in colour. Blue crystals of sapphirine and dark green spinel are recognized in hand specimen (Fig. 2g). The calc-granulite is interbanded with khondalite and is usually banded, and it is marked by grooved surfaces on weathered outcrops (Fig. 2h). The most abundant planar features of the various metamorphic rocks in the study area are foliations. From the orientation pattern of the foliations in three structurally similar sub-areas and corresponding β-maxima in stereograms (Fig. 3), refolding of the syn-metamorphic foliation during a later deformational event is evident.

4. Petrography

4.a. Charnockite, enderbite and mafic granulite

All of these rocks are characterized by a granoblastic texture formed by a mosaic of garnet, orthopyroxene, plagioclase, quartz and K-feldspar. Garnet occurs as coarse- to fine-grained anhedral to euhedral crystals. Inclusions of quartz, biotite, plagioclase and ilmenite

https://doi.org/10.1017/S0016756814000399 Published online by Cambridge University Press

Figure 2. (Colour online) Field photographs of the principal rock types in the study area: (a) Massive charnockite exposure with greasy look due to predominance of grey quartz with waxy lustre and dark brown garnet; (b) black to dark grey mafic granulite; dark patches are rich in ferromagnesian minerals; (c) grey leptynite with high proportion of finely dispersed, small garnet grains; (d) yellowish weathered leptynite with large garnet accumulations (dark red-brown); (e) medium- to coarse-grained, yellowish-greyish weathered khondalite; (f) banded migmatite with a separation into restitic and coarse-grained quartzo-feldspathic leucosome layers; (g) sapphirine–spinel-bearing granulite with bluish crystals of sapphirine and dark green spinel; (h) calc-silicate rock with serrated pattern due to differential weathering.

https://doi.org/10.1017/S0016756814000399 Published online by Cambridge University Press

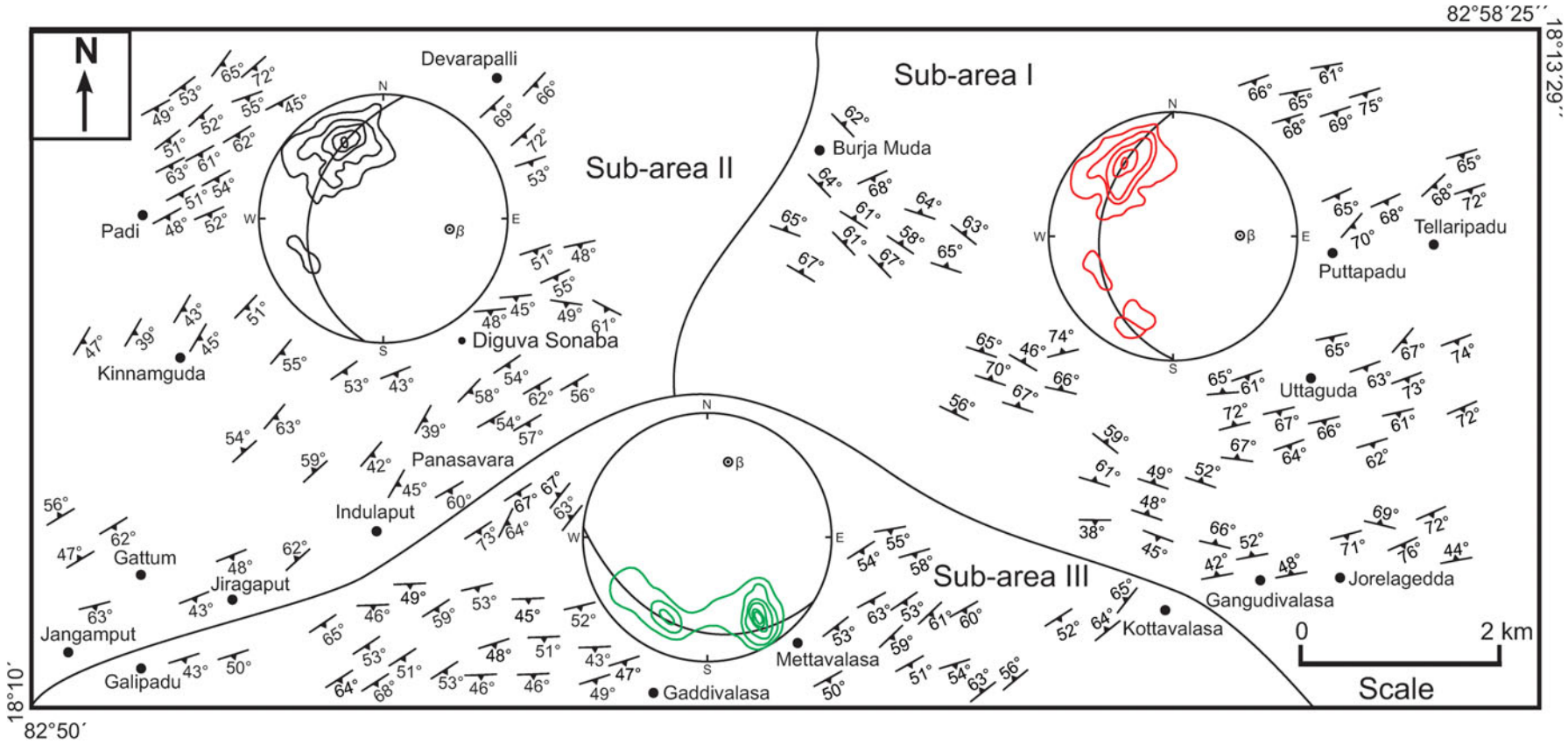

Figure 3. (Colour online) Structural map of the study area showing prominent S-surfaces (foliation) along with lower hemisphere of equal area projection of poles (N = 161) to foliation (contour interval: 3, 6, 9 and 12 % per 1 % area). The blocks demarcated by continuous lines correspond to sub-areas.

are present in garnet (Fig. 4a), suggesting the prograde reaction

$$2\ \text{biotite} + 6\ \text{quartz} = \text{garnet} + \text{orthopyroxene} + 2\ \text{K-feldspar} + 2\ H_2O \quad (1)$$

Secondary biotite rimming garnet, orthopyroxene and K-feldspar in the garnet enderbite and charnockite indicates that Reaction (1) also took place in the retrograde direction.

Hornblende occurs as both prograde and retrograde generation. In the mafic granulite relict hornblende occurs as inclusions within pyroxenes, suggesting the prograde reaction

$$2\ \text{hornblende} + 8\ \text{quartz} = 3\ \text{orthopyroxene} + 2\ \text{clinopyroxene} + 4\ \text{plagioclase} + 2\ H_2O \quad (2)$$

whereas retrograde hornblende occurs as rims around ortho- and clinopyroxene (Fig. 4d), indicating that Reaction (2) was partially reversed during retrograde overprint.

Accessory minerals include magnetite, ilmenite, apatite, titanite, spinel and pyrrhotite. Magnetite occurs as elongated grains in the matrix and also along the cleavage planes in pyroxenes and biotite.

4.b. Leptynite and khondalite

Leptynite and garnet-leptynite exhibit a mostly granoblastic texture defined by an interlocking arrangement of quartz, K-feldspar, plagioclase and garnet. Myrmekitic intergrowths of quartz and plagioclase, and perthitic and antiperthic intergrowths in feldspars are common. With gradually increasing content of biotite, leptynite changes into biotite-gneisses (± garnet).

Garnet typically occurs as medium- to coarse-grained xenoblasts in khondalite. Poikiloblastic garnet contains inclusions of quartz, sillimanite and spinel (Fig. 4e). Retrograde biotite occurs along fractures and rims of garnet (Fig. 4f). Symplectites of secondary garnet II + quartz form rims around xenoblasts of garnet I (Fig. 4g).

In both the khondalite and leptynite, rounded blebs of biotite and subangular quartz grains occur within garnet and also within perthite that is present in the matrix. This textural relationship may be due to the reaction

$$\text{biotite} + \text{quartz} = \text{garnet} + \text{K-feldspar} + H_2O \quad (3)$$

In the sillimanite-bearing assemblages, sillimanite occurs, together with biotite and quartz, also as inclusions in garnet and K-feldspar, which may be attributed to the reaction

$$\text{biotite} + \text{sillimanite} + 2\ \text{quartz} = \text{garnet} + \text{K-feldspar} + H_2O \quad (4)$$

Coarse-grained biotite and biotite–quartz symplectites and sillimanite rimming xenoblasts of garnet (Fig. 4h) presumably formed owing to retrograde hydration through reversal of reactions (3) and (4).

4.c. Sapphirine and/or spinel-bearing granulite

4.c.1. Sapphirine-bearing granulite without spinel

Aggregates of sillimanite (up to 0.8 mm in length), which mimic the shape and simple twinning of coarse-grained kyanite blades (Fig. 5a), have been interpreted as pseudomorphs after kyanite (Lal *et al.* 1984; Raith, Karmakar & Brown, 1997; Brandt *et al.* 2011). This implies a prograde assemblage of biotite–orthopyroxene–garnet–plagioclase–kyanite, and a peak metamorphic assemblage of orthopyroxene–garnet–sillimanite–alkali feldspar–rutile–quartz.

The post-peak mineral assemblages are represented by various types of reaction coronas. These coronas occur within a matrix of cordierite, quartz, K-feldspar and plagioclase. The corona includes the following types (minerals arranged from core to rim): (a) sapphirine–sillimanite–cordierite (Fig. 5b); (b) sapphirine–cordierite–orthopyroxene (Fig. 5c, d); (c) sapphirine–sillimanite–orthopyroxene (Fig. 5e), in which sapphirine is separated from quartz by successive reaction coronas of sillimanite and orthopyroxene; and (d) sapphirine–sillimanite–cordierite–orthopyroxene. Other assemblages include: sapphirine–cordierite symplectites, orthopyroxene–cordierite symplectites (Fig. 5f), cordierite–orthopyroxene–K-feldspar–quartz (Fig. 5g), and coarse-grained orthopyroxene–sillimanite–K-feldspar–quartz (Fig. 5h), which form symplectitic intergrowths.

4.c.2. Spinel-bearing granulite without sapphirine

This rock type can contain three different mineral assemblages, each characterized by specific types of corona.

The paragenesis spinel–sillimanite–cordierite–quartz–orthopyroxene–magnetite displays, in places, spinel–magnetite–sillimanite–orthopyroxene coronas in which spinel with exsolved magnetite is successively mantled by sillimanite and orthopyroxene in a matrix of quartz (Fig. 6a). Where the peak metamorphic mineral assemblage is spinel–magnetite–sillimanite, spinel is isolated from cordierite (Fig. 6b). Other minerals that form symplectites around spinel include orthopyroxene–sillimanite–cordierite (Fig. 6c).

In the assemblage spinel–garnet–K-feldspar ± phlogopite ± sillimanite, garnet and K-feldspar occur as inclusions in spinel.

4.c.3. Sapphirine–spinel-bearing granulite

Two types of this rock are distinguished:

(1) A granulite with the paragenesis sapphirine, spinel, orthopyroxene, cordierite, quartz, sillimanite, (cordierite–orthopyroxene–K-feldspar–quartz)-bearing symplectite ± plagioclase, magnetite, rutile, zircon and lamellar intergrowths of haematite–ilmenite.

This rock displays a number of reaction coronas and the minerals present in them constitute the

https://doi.org/10.1017/S0016756814000399 Published online by Cambridge University Press

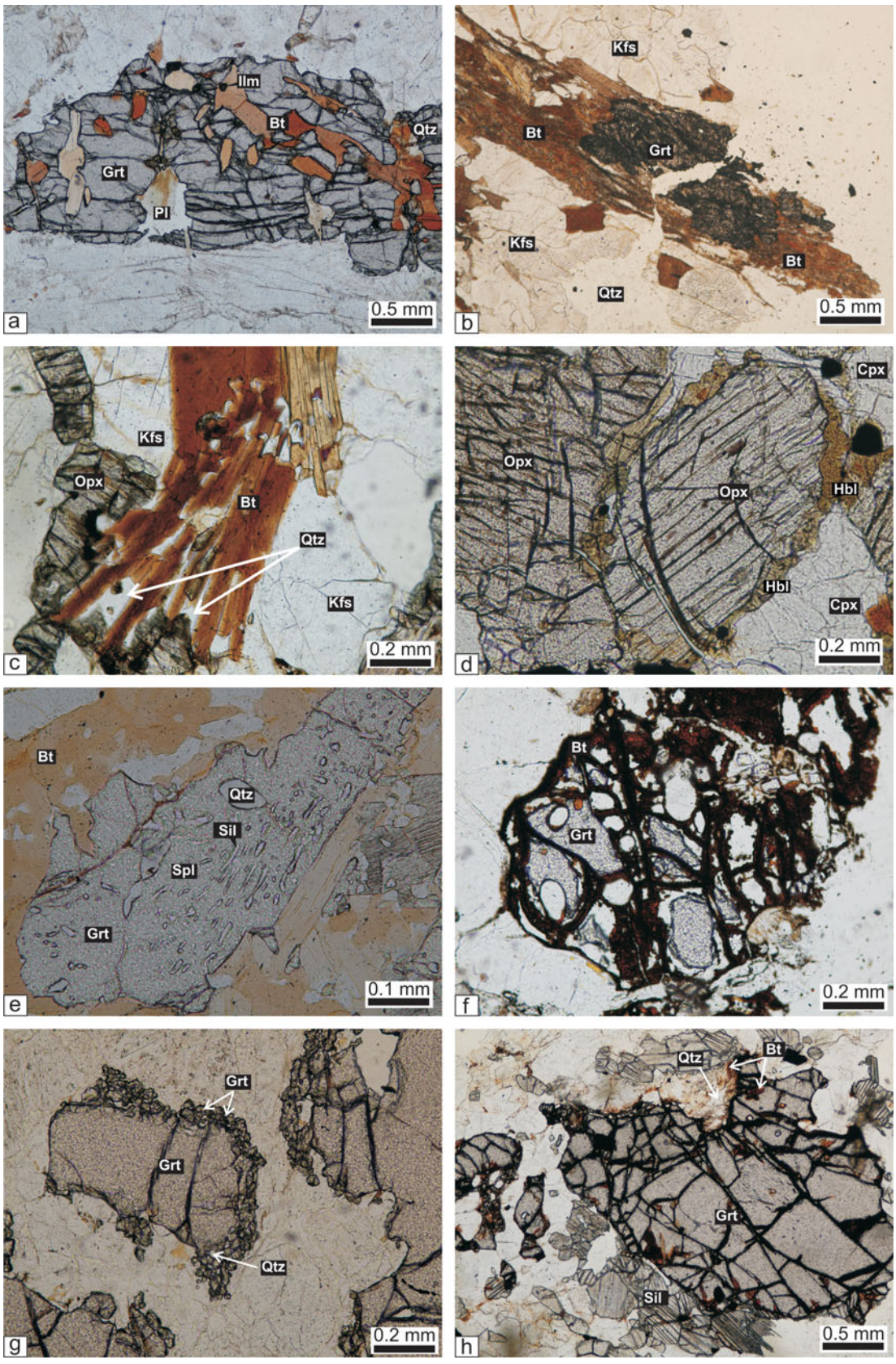

Figure 4. (Colour online) Photomicrographs of charnockite, mafic granulite, khondalite and leptynite examined in this study. (a) Quartz, biotite, plagioclase and ilmenite occurring as inclusions in garnet porphyroblasts (sample no. 1113); (b) biotite rims around corroded garnet (sample no. 1113); (c) biotite–quartz symplectite around orthopyroxene and K-feldspar (sample no. 1113); (d) hornblende around orthopyroxene and clinopyroxene (sample no. 1101); (e) poikiloblastic garnet containing inclusions of quartz, sillimanite and spinel (sample no. 1100); (f) biotite along fractures and rims of relict garnet (sample no. 1105); (g) presence of comparatively small second-generation garnet with quartz around xenoblasts of garnet (sample no. 1100); (h) development of sillimanite and biotite–quartz symplectites around corroded garnet porphyroblast (sample no. 1100).

https://doi.org/10.1017/S0016756814000399 Published online by Cambridge University Press

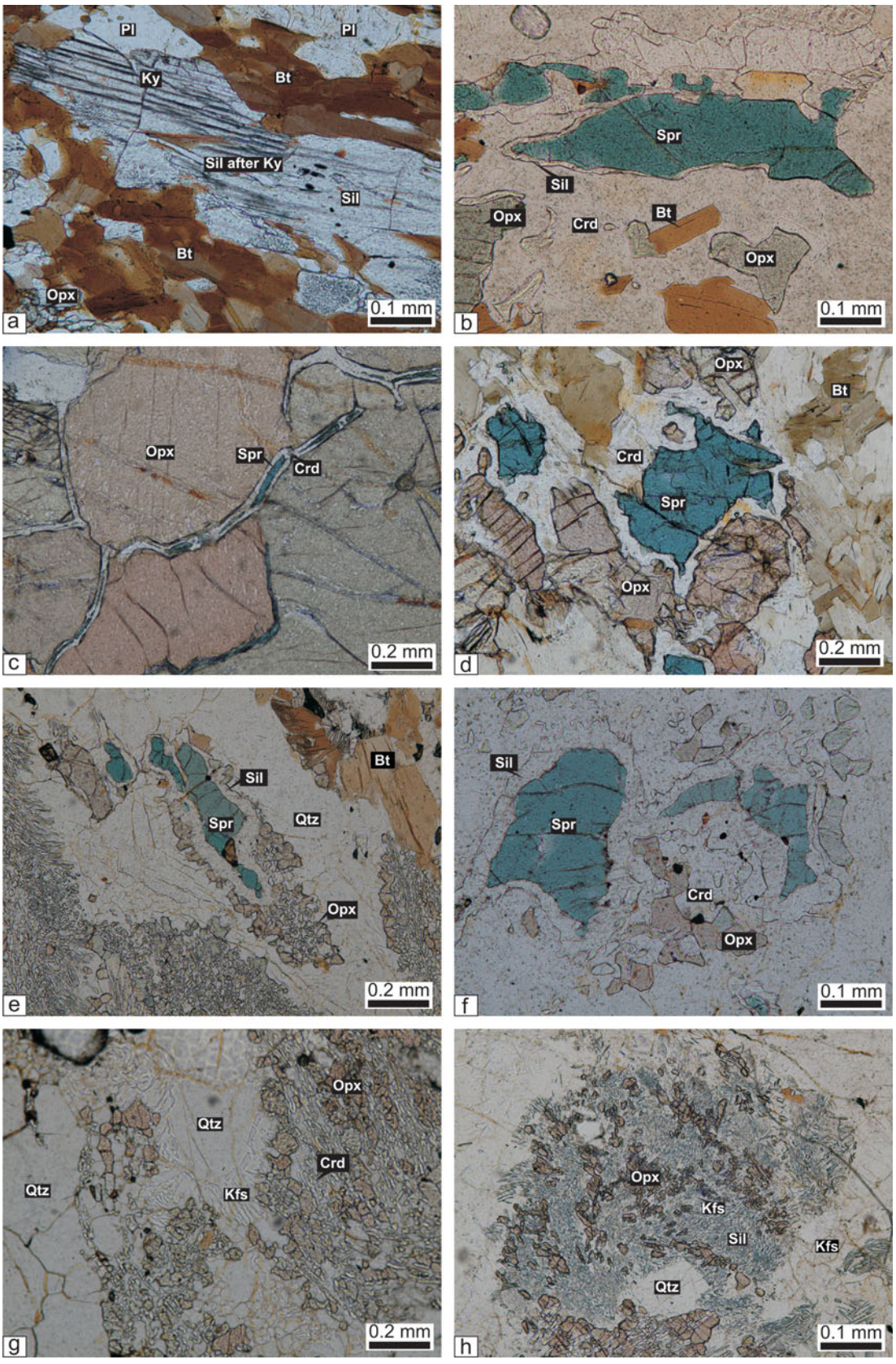

Figure 5. (Colour online) Photomicrographs of sapphirine-bearing granulite without spinel: (a) polycrystalline aggregate of sillimanite pseudomorphs after coarse blades of earlier kyanite (sample no. 1111); (b) sapphirine rimmed by sillimanite in matrix of cordierite (sample no. 1111); (c) radial replacement of orthopyroxene by sapphirine mantled by cordierite (sample no. 1111); (d) sapphirine separated from orthopyroxene by cordierite (sample no. 1111); (e) sapphirine separated from quartz by a moat of sillimanite and orthopyroxene (sample no. 1112); (f) sapphirine in a matrix of symplectitic intergrowth of orthopyroxene and cordierite (sample no. 1107); (g–h) orthopyroxene–cordierite/sillimanite–K-feldspar–quartz symplectite, which possibly formed from the breakdown of osumilite (sample no. 1112).

https://doi.org/10.1017/S0016756814000399 Published online by Cambridge University Press

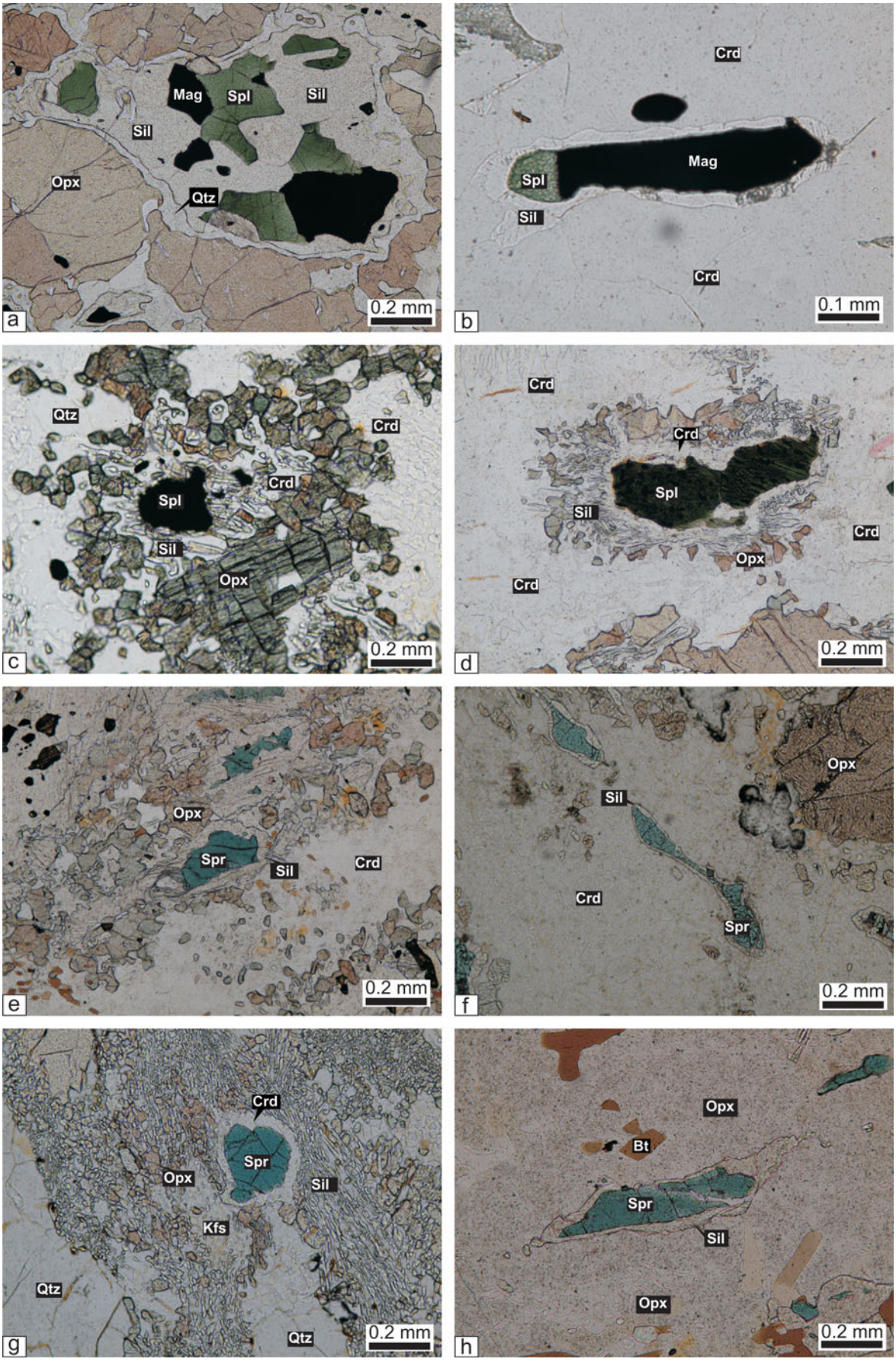

Figure 6. (Colour online) Photomicrographs of spinel-bearing granulite without sapphirine (a–c) and of sapphirine–spinel-bearing granulite (d–h): (a) spinel and successively rimmed by sillimanite, quartz and orthopyroxene (sample no. 1122); (b) spinel and magnetite rimmed by sillimanite in the matrix of cordierite (sample no. 1122); (c) spinel and quartz are isolated from each other by orthopyroxene–cordierite–sillimanite symplectitic intergrowth (sample no. 1122); (d) spinel is successively rimmed by cordierite,

https://doi.org/10.1017/S0016756814000399 Published online by Cambridge University Press

following mineral assemblages: (a) spinel–sillimanite–cordierite–orthopyroxene (Fig. 6d); (b) sapphirine–sillimanite–cordierite–orthopyroxene (Fig. 6e); (c) sapphirine–sillimanite–cordierite (Fig. 6f); (d) sapphirine–cordierite mantled by symplectites of orthopyroxene, sillimanite, quartz and K-feldspar (Fig. 6g); (e) sapphirine–sillimanite–orthopyroxene (Fig. 6h); (f) sapphirine–spinel–magnetite–rutile–ilmenite–haematite–sillimanite–orthopyroxene (Fig 7a); (g) spinel–sapphirine–sillimanite–orthopyroxene–quartz–K-feldspar (Fig. 7b); (h) (spinel–sapphirine)–cordierite–orthopyroxene (Fig. 7c). These coronas commonly occur in the matrix of quartz and symplectites of cordierite–orthopyroxene–K-feldspar–quartz. In places, coronas are present within the matrix of this symplectite only.

(2) The second variety is made up of sapphirine, spinel, garnet, sillimanite, phlogopite, quartz and K-feldspar, with accessory ilmenite and zircon. The rock contains the following types of coronas: (a) spinel–sapphirine in garnet (Fig. 7d); (b) spinel–sapphirine inclusions in quartz (Fig. 7e); (c) spinel–sapphirine inclusions in sillimanite (Fig. 7f); and (d) spinel–sapphirine–cordierite–garnet.

In the assemblage spinel–garnet–phlogopite–quartz–magnetite–ilmenite, spinel/sapphirine occurs in contact with quartz (Fig. 7e, g).

The textural relationships of the different minerals present in the above rock types are summarized as follows:

Two textural types of orthopyroxene are present. An older generation of orthopyroxene I is coarse grained and anhedral to subhedral (up to 2 cm in length). Prograde corroded biotite (phlogopite) occurs as inclusions in this orthopyroxene. The second generation of orthopyroxene is fine to medium grained, anhedral and forms coronas with spinel, sapphirine, sillimanite and cordierite. It also occurs as finger-like trails in symplectitic intergrowths of cordierite–orthopyroxene–K-feldspar–quartz and orthopyroxene–sillimanite–quartz ± K-feldspar (Fig. 5g, h).

Cordierite occurs in various types of coronas around sillimanite, sapphirine, spinel and orthopyroxene. Cordierite also forms symplectitic intergrowths with orthopyroxene, K-feldspar and quartz (Fig. 5g).

Like cordierite and orthopyroxene, two generations of sillimanite are present. Sillimanite I is not involved in the formation of corona structures and the symplectitic intergrowths. It occurs as coarse prismatic grains or needles in association with coarse-grained orthopyroxene. Sillimanite II is observed in coronas around sapphirine and spinel (Figs 5b, 7b). In some samples sillimanite II also forms symplectitic intergrowths with orthopyroxene, K-feldspar and quartz (Fig. 5h).

Sapphirine occurs in grain contact with quartz, which indicates that sapphirine + quartz was stable during the thermal peak of metamorphism (Fig. 7g). In other samples, sapphirine and quartz are separated by retrograde corona rims. The presence of ilmenite–haematite intergrowths within spinel, particularly where it mantles sapphirine (Fig. 7a, b), suggests high oxygen fugacity during the formation of the reaction coronas involving sapphirine, spinel, sillimanite and orthopyroxene.

In most of the samples, spinel is fine grained, green in colour and anhedral. In a few samples it is intergrown with magnetite suggesting mutual exsolution (Fig. 6a, b). In most of the samples, spinel occurs in the cores of sapphirine and forms intergrowths with magnetite and K-feldspar (Fig. 7b).

In one sample (no. 1110), garnet occurs in the corona where spinel is successively rimmed by sapphirine and garnet in a matrix of quartz. This textural relationship may be explained by the reaction

$$10\ \text{spinel} + 6\ \text{quartz} = \text{garnet} + 2\ \text{sappirine}_{(7:9:3)} \qquad (5)$$

Although osumilite could not be identified in the sapphirine–spinel-bearing rocks, its crystallization during the thermal peak of metamorphism is suggested by the common occurrence of symplectitic intergrowth of cordierite–orthopyroxene–K-feldspar–quartz, which is a breakdown product of osumilite through the reaction

$$3\ \text{osumilite} = 2\ \text{cordierite} + \text{orthopyroxene} + 3\ \text{K - feldspar} + 7\ \text{quartz} \qquad (6)$$

The breakdown of osumilite to this type of symplectite was first suggested by Schreyer & Seifert (1967) and has since been reported by several workers (Berg & Wheeler, 1976; Ellis, 1980; Grew, 1982; Lal, Ackermand & Upadhyay, 1987; Nowicki, Frimmel & Waters, 1995; Bhattacharya & Kar, 2002; Adjerid *et al.* 2013). In some samples the symplectite pseudomorphs after osumilite are devoid of cordierite and contain orthopyroxene–K-feldspar–sillimanite–quartz, which may be related to the reaction

$$\text{osumilite} = \text{orthopyroxene} + \text{K - feldspar} + 2\ \text{sillimanite} + 3\ \text{quartz} \qquad (7)$$

4.d. Calc-granulite

This rock consists mainly of diopside, calcite, scapolite, wollastonite and plagioclase. Diopside occurs as medium to coarse grained, in places poikiloblastic, grains

sillimanite and orthopyroxene (sample no. 1108); (e) sapphirine is successively rimmed by sillimanite and fine-grained orthopyroxene aggregates in a matrix of cordierite (sample no. 1102); (f) sapphirine is completely rimmed by sillimanite in the matrix of cordierite (sample no. 1102); (g) sapphirine rimmed by cordierite in a matrix of symplectitic intergrowth of orthopyroxene–sillimanite–K-feldspar–quartz (sample no. 1102); (h) sapphirine completely rimmed by sillimanite within orthopyroxene (sample no. 1102).

https://doi.org/10.1017/S0016756814000399 Published online by Cambridge University Press

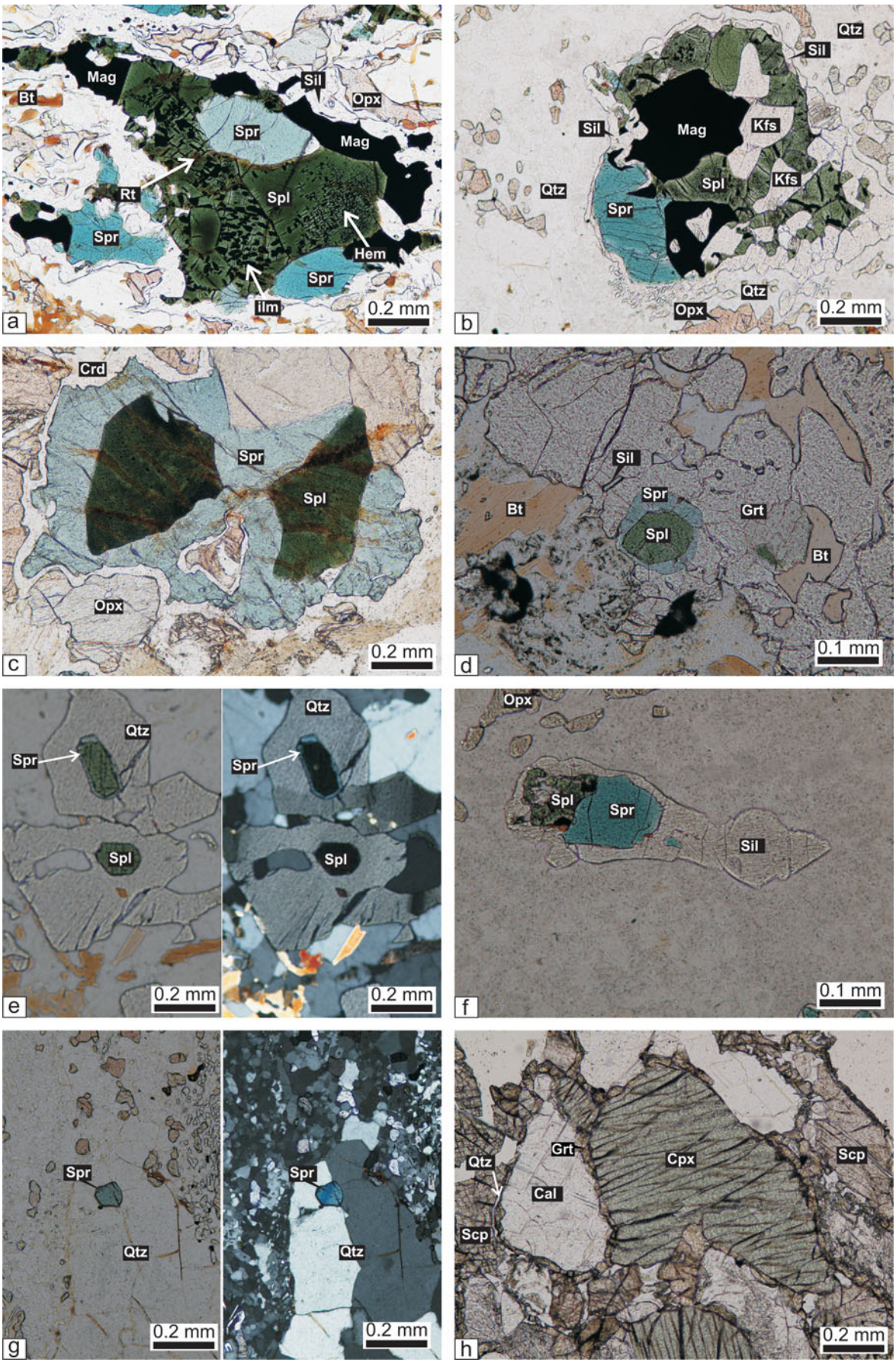

Figure 7. (Colour online) Photomicrographs of sapphirine–spinel-bearing granulite: (a) rutile–ilmenite–haematite lamellae within spinel (sample no. 1104); (b) sapphirine, magnetite and spinel rimmed by sillimanite in the matrix of quartz (sample no. 1104); (c) spinel and sapphirine successively rimmed by cordierite and orthopyroxene (sample no. 1110); (d) spinel rimmed by sapphirine within garnet (sample no. 1110); (e) spinel in grain contact with quartz (both in plain-polarized light and cross-polarized light) (sample no.

https://doi.org/10.1017/S0016756814000399 Published online by Cambridge University Press

that contain numerous inclusions of quartz, plagioclase, scapolite, titanite, spinel, magnetite and biotite. Calcite is mostly coarse grained, subidioblastic to xenoblastic. Fine-grained xenoblastic calcite occurs with fine-grained quartz aggregates. Fine-grained calcite occurs as inclusions in diopside and vesuvianite. The association of wollastonite with calcite or quartz is explained by the reaction

$$\text{calcite} + \text{quartz} = \text{wollastonite} + CO_2 \quad (8)$$

Grossular occurs as medium- to coarse-grained xenoblasts. It mostly forms a corona rim along with quartz between diopside and scapolite (Fig. 7h), which suggests the following reaction

$$\text{diopside} + \text{scapolite} = \text{grossular} + \text{quartz} \quad (9)$$

Grossular also forms rims between calcite and scapolite (Fig. 7h) suggesting the reaction

$$5\ \text{calcite} + \text{scapolite} + 3\ \text{quartz} = 3\ \text{grossular} + 6\ CO_2 \quad (10)$$

5. Mineral chemistry

Electron microprobe analyses (EMPA) were carried out on an automated energy-dispersive electron microanalyser JEOL JSM-5300 and LINK QX2000J system, operated at an acceleration voltage of 15 kV and a specimen current of 15 nA at the Geological Institute, Yokohama National University, Japan. Analyses were refined using the LINK ZAF-4/FLS correction program. Eleven representative samples were chosen for detailed mineral chemical analyses. Routine detection limits are in the order of 0.008 wt % for most elements. The representative microprobe analyses of the analysed minerals are listed in Tables S1–10 in the online Supplementary Material available at http://journals.cambridge.org/geo. Mineral abbreviations used are taken from Kretz (1983).

5.a. Garnet

Garnet in the different rock types is essentially a solid solution of almandine, pyrope and grossular, with minor spessartine (Fig. 8a; Table S1 in the online Supplementary Material available at http://journals.cambridge.org/geo).The pyrope content in the garnet is highest in sapphirine–spinel granulite, followed by garnet-leptynite, khondalite and mafic granulite. The X_{Mg} ranges from 0.30 to 0.54 in Grt–Spr–Spl–Sil-Qtz coronas, 0.48 to 0.51 in Grt–Opx–Sil–Qtz coronas and 0.47 to 0.50 in Grt–Phl–Crd–Qtz coronas.

5.b. Biotite

In general, biotite is most magnesian (X_{Mg} = 0.78–0.94) in sapphirine–spinel granulite whereas in mafic granulite and garnet-leptynite it has lower X_{Mg} of 0.40–0.89 and 0.55–0.71, respectively (Table S2 in the online Supplementary Material available at http://journals.cambridge.org/geo). The TiO_2 contents of biotite in the sapphirine–spinel granulites are between 1.13 and 5.23 wt %, in the garnet-leptynites between 2.57 and 4.99 wt %, and in the mafic granulites between 0.67 and 3.64 wt %.

5.c. Sapphirine

In the triangular diagram $(Al,Fe,Cr)_2O_3$–MgO + FeO–SiO_2 (Fig. 8c), the analysed sapphirine grains (Table S3 in the online Supplementary Material available at http://journals.cambridge.org/geo) plot between the 7:9:3 and 2:2:1 but close to the 7:9:3 position. Those analyses that plot between 7:9:3 and 3:5:1 of the solid solution series are peraluminous. The X_{Mg} ratio of sapphirine ranges from 0.72 to 0.83. The number of silicon atoms related to 18 oxygens varies in different coronas, i.e. 0.69–0.76 p.f.u. in the Spl–Spr–Qtz coronas, 0.81–0.84 in the Grt–Spr–Spl–Qtz and 0.81–0.87 in the Spl–Spr–Sil–Opx–Qtz coronas. Correspondingly, Al^{VI} is highest in Spr–Spl–Qtz and lowest in Spl–Spr-Sil–Opx–Qtz coronas. Moreover, the cores of sapphirine grains are less aluminous than their rims. Total FeO varies from 7.8 to 12.9 wt % and the Fe^{3+} content of sapphirine increases from the Spl–Spr–Qtz (0.05 p.f.u.) via the Spl–Spr–Opx–Sil (0.07 p.f.u.) to the Grt–Spr–Spl–Qtz coronas (up to 0.15 p.f.u.). With few exceptions, TiO_2 in sapphirine is below the detection limit, while Cr_2O_3 can reach as much as 0.87 and MnO as much as 0.36 wt %.

5.d. Pyroxenes

Most of the mafic granulite samples (nos 1101, 1103, 1106) contain pairs of coexisting clinopyroxene (hedenbergite to diopside with X_{Mg} 0.44–0.58) and orthopyroxene (ferrosilite with X_{Mg} 0.33–0.38) and Al_2O_3 contents of 0.48–0.80 wt % (Table S4 in the online Supplementary Material available at http://journals.cambridge.org/geo; Fig. 8d). Samples no. 1101 and 1106 contain diopside with X_{Mg} of 0.50–0.58 that does not coexist with orthopyroxene. In contrast, enstatite is the only pyroxene in the other granulite types. Sapphirine-bearing granulite contains orthopyroxene with high Al_2O_3 contents of 5.39–9.78 wt %, whereas, in charnockites, the Al_2O_3 content is distinctly lower, ranging from 1.25 to 1.54 wt %. The

1108); (f) sapphirine and spinel inclusion within sillimanite (sample no. 1108); (g) sapphirine in grain contact with quartz (both in plain-polarized light and cross-polarized light) (sample no. 1108); (h) calc-granulite showing granoblastic microstructure. Grossular forms a reaction rim between calcite, clinopyroxene and scapolite (sample no. 1109); Bt – biotite; Cal – calcite; Cpx – clinopyroxene; Crd – cordierite; Grt – garnet; Hbl – hornblende; Ilm – ilmenite; Kfs – K-feldspar; Ky – kyanite; Mag – magnetite; Opx – orthopyroxene; Pl – plagioclase; Qtz – quartz; Rt – rutile; Scp – scapolite; Sil – sillimanite; Spl – spinel; Spr – sapphirine.

https://doi.org/10.1017/S0016756814000399 Published online by Cambridge University Press

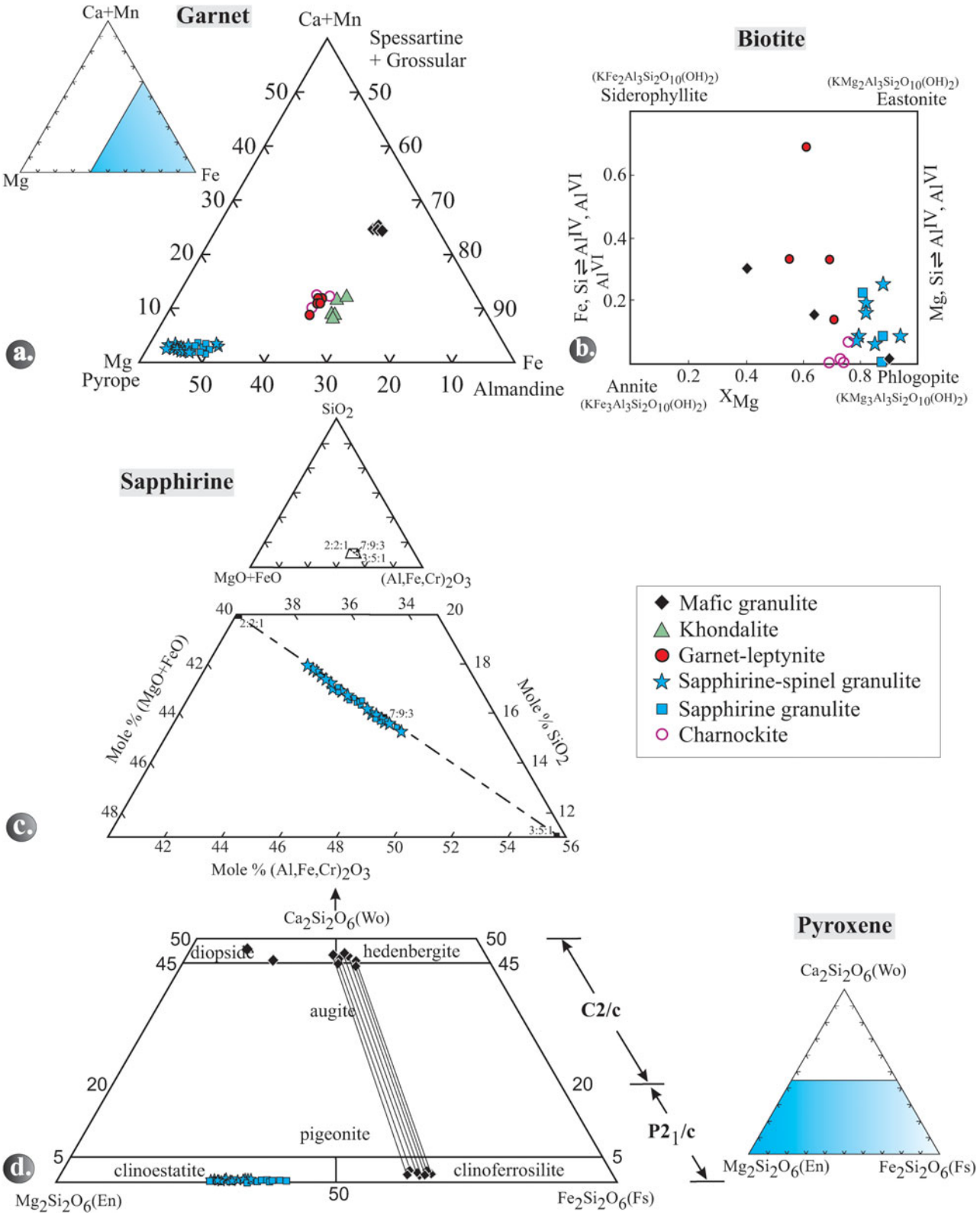

Figure 8. (Colour online) (a) Triangular diagram showing the variation in spessartine + grossular–almandine–pyrope end-member proportions in garnet in the various rock types. (b) Quadrangular diagram showing the variation in annite–phlogopite–siderophyllite–eastonite end-member proportions in biotite in the various rock types. (c) A part of the system SiO_2–(FeO + MgO)–$(Al,Fe,Cr)_2O_3$ showing plots of the analysed sapphirine. Solid rectangles with numbers 2:2:1, 7:9:3 and 3:5:1 give molar ratios for the ternary composition in the order (FeO + MgO) + $(Al,Fe,Cr)_2O_3$ + SiO_2. (d) Pyroxene quadrilateral showing the composition of ortho- and clinopyroxenes from different rock types. Tie lines represent pairs of coexisting pyroxenes.

https://doi.org/10.1017/S0016756814000399 Published online by Cambridge University Press

trend of X_{Mg} of orthopyroxene in the rock types is as follows: sapphirine granulite (0.59–0.72), sapphirine–spinel granulite (0.55–0.72) and mafic granulite (0.33–0.38). The highest X_{Mg} is observed in orthopyroxene from garnet–orthopyroxene domains (0.62–0.72), followed by sapphirine–spinel–orthopyroxene–sillimanite domains (0.66–0.68) and orthopyroxene–cordierite–spinel domains (0.53–0.69).

5.e. Cordierite

The majority of the analysed cordierite grains (Table S5 in the online Supplementary Material available at http://journals.cambridge.org/geo) are highly magnesian (X_{Mg} = 0.80–0.92). No significant zoning was observed. Insignificant amounts of CaO and K_2O are present (up to 0.4 and 0.6 wt %, respectively), whereas Na_2O is below the detection limit. Except in a few cases, the totals are close to 100 wt %, which indicates that these are essentially anhydrous cordierite grains. Some analyses yielded lower totals, and this is likely due to the presence of some H_2O and/or CO_2 (Hörmann *et al.* 1980; Lonker, 1981).

5.f. Plagioclase

Judging from the $Ca/(Ca + Na + K) \times 100$ values, the An contents of plagioclase (Table S6 in the online Supplementary Material available at http://journals.cambridge.org/geo) range from 43 to 75 mol % in the mafic granulites, from 35 to 54 mol % in garnet-leptynite and from 35 to 43 mol % in the sapphirine–spinel granulites.

5.g. K-feldspar

The albite content ($(Na/(Ca + Na + K)) \times 100$) ranges between 10 and 22 mol % in the sapphirine–spinel granulite, between 8 and 13 mol % in the khondalite, and it is approximately 10 % in the garnet-leptynite and 8 % in the mafic granulite (Table S7 in the online Supplementary Material available at http://journals.cambridge.org/geo). Iron (calculated as Fe_2O_3) may be present up to 0.18 wt %, but is in most cases below the detection limit. The same holds true for TiO_2, Cr_2O_3, MnO and MgO.

5.h. Sillimanite

Most of the sillimanite grains recorded in a few samples contain considerable amounts of Fe_2O_3 ranging up to 0.86 wt % in sapphirine granulites and from 0.76 to 1.51 wt % in sapphirine–spinel-orthopyroxene–quartz granulites (Table S8 in the online Supplementary Material available at http://journals.cambridge.org/geo). This variation in Fe_2O_3 suggests differences in oxidizing conditions during metamorphism. With one exception, Cr_2O_3 is below the detection limit; TiO_2, MnO and MgO could not be detected.

5.i. Spinel

Spinel is largely a solid solution between spinel ($MgAl_2O_4$) and hercynite ($Fe^{2+}Al_2O_4$) with X_{Mg} ranging from 0.29 to 0.60 and also some $Al–Fe^{3+}$ substitution (Table S9 in the online Supplementary Material available at http://journals.cambridge.org/geo). Cr_2O_3 and MnO are present in minor amounts and, with few exceptions, TiO_2 and ZnO are below the detection limit. X_{Mg} is at 0.43–0.56 in Spl–Spr–Sil–Opx coronas, 0.44–0.56 in Spl–Spr–Grt coronas, 0.29–0.48 in Spl–Opx–Sil–Crd coronas and 0.36 in spinel–biotite associations. Spinel coexisting with magnetite shows low Al_2O_3 and, consequently, higher Fe^{3+} contents (cf. Ackermand *et al.* 1987).

5.j. Ilmenite, Ilmeno-haematite and haematite

The opaque minerals recorded in the granulites investigated include magnetite, ilmenite, ilmenite–haematite solid solutions, haematite and rutile. The sapphirine–spinel granulites contain ilmenite with about 5 mol % Fe_2O_3, but also ilmeno-haematite with 55–70 mol % Fe_2O_3, as well as nearly pure haematite (Table S10 in the online Supplementary Material available at http://journals.cambridge.org/geo).

6. Chemographic relationships and metamorphic reactions

The sapphirine–spinel granulite (as exemplified by sample no. 1110) is particularly useful for petrological modelling because it contains the three-phase assemblage orthopyroxene–sapphirine–spinel in the $(MgO + FeO)–(Al_2O_3 + Fe_2O_3 + Cr_2O_3)–SiO_2$ model system (Fig. 9).

6.a. Reactions in sapphirine–spinel granulite

Spinel, partially or wholly rimmed by sapphirine, occurs along the interstices of coarse prismatic aggregates of orthopyroxene. This textural relationship may be attributed to the reaction

$$5\ \text{Mg - tschermakite} + 4\ \text{spinel} = 2\ \text{sapphirine}_{(7:9:3)} + \text{enstatite} \quad (11)$$

(in orthopyroxene).

The composition of sapphirine lies in the three-phase field of the spinel–sillimanite–quartz reaction:

$$7\ \text{spinel} + 2\ \text{sillimanite} + \text{quartz} = 2\ \text{sappirine}_{(7:9:3)} \quad (12)$$

Co-linear positions of the three phases point to degenerated systems with the three-phase reactions

$$2\ \text{spinel} + 5\ \text{quartz} = \text{cordierite} \quad (13)$$

and

$$\text{sapphirine}_{(2:2:1)} + 8\ \text{quartz} = 2\ \text{cordierite} \quad (14)$$

https://doi.org/10.1017/S0016756814000399 Published online by Cambridge University Press

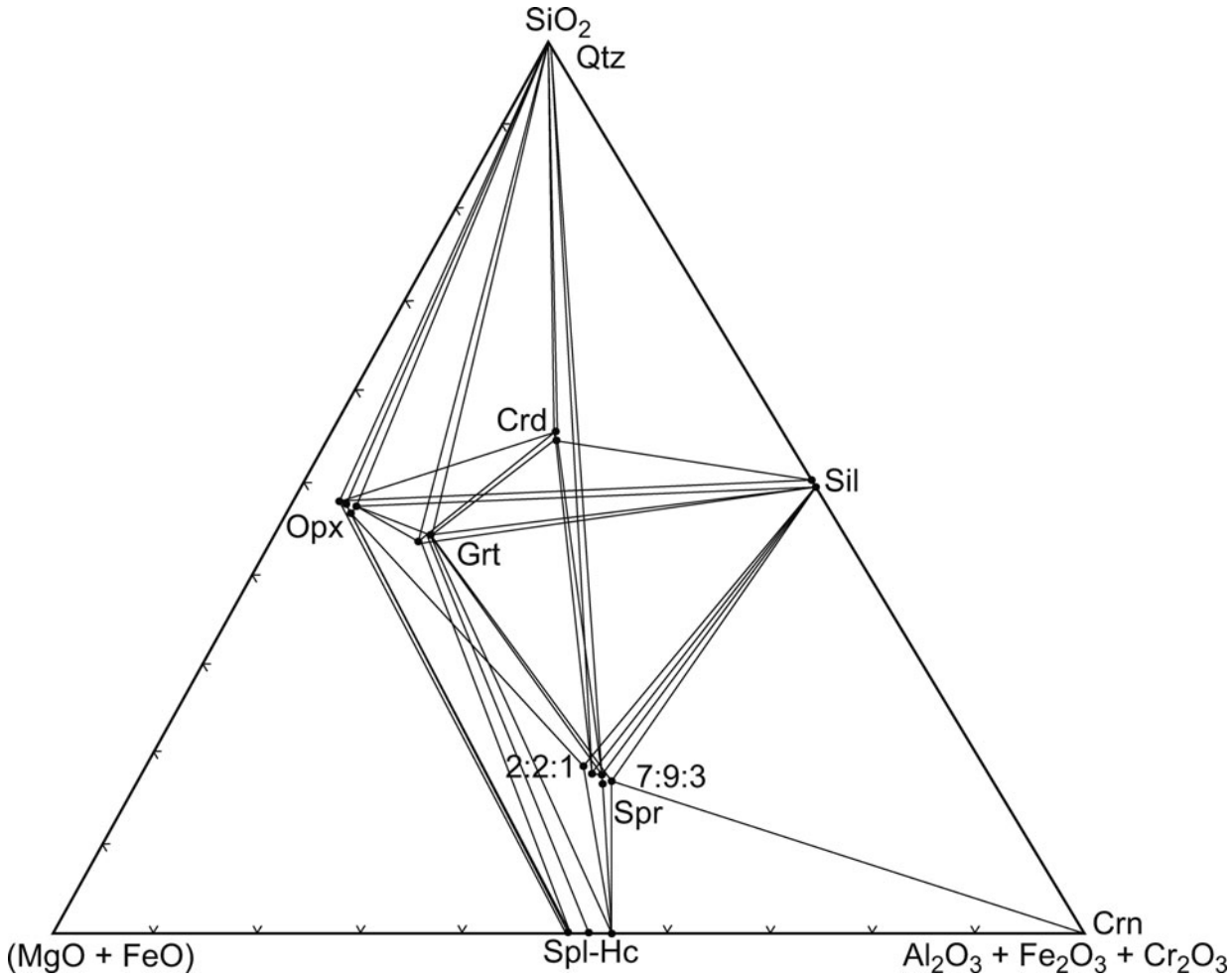

Figure 9. $(Mg–Fe^{2+})O–(Al,Fe^{3+},Cr)_2O_3–SiO_2$ diagram showing the composition of coexisting minerals in the sapphirine–spinel-bearing granulites. Crossed tie lines reflect the higher variance of the assemblages due to the fractionation of Mg and Fe^{2+} as well as Al, Cr, Fe^{3+} among the phases.

The phase relations can be displayed in the model system $K_2O–FeO–MgO–A1_2O_3–SiO_2–H_2O$ (KFMASH) in which FeO and MgO are treated as separate components. This can be simplified by excluding the following minerals:

(1) Osumilite, though present at the thermal peak of metamorphism, has been completely replaced by symplectite of orthopyroxene–quartz–K-feldspar–cordierite;

(2) K-feldspar is ubiquitous and thus can be treated as an excess phase; and

(3) biotite, because it was involved predominantly in retrograde reactions.

As most of the sapphirine and spinel-bearing assemblages of the study area contain sillimanite, the phase relations can be shown in plane projection from sillimanite onto the $SiO_2–FeAl_2O_4–MgAl_2O_4$ plane of the $FeO–MgO–A_2O_3–SiO_2$ tetrahedron (Fig. 10). A plausible sequence of metamorphic reactions, based upon the textural relationships, is shown in a series of sillimanite projections (Fig. 10).

The sequence of reaction coronas in these rocks indicates earlier stability of sapphirine + quartz and spinel + quartz during the thermal peak of metamorphism. Experimental work in the $MgO–Al_2O_3–SiO_2–H_2O$ (MASH) and $FeO–MgO–Al_2O_3–SiO_2–H_2O$ (FMASH) systems has demonstrated the stability of the association sapphirine + spinel with quartz at high-pressure – high-temperature conditions (Schreyer & Seifert, 1969; Hensen & Green, 1971; Chatterjee & Schreyer, 1972). The spinel–sapphirine–(garnet + sillimanite) corona in sample no. 1110 may be attributed to a discontinuous Fe^{2+}–Mg reaction (Fig. 10a, b):

$$13 \text{ spinel} + 11 \text{ quartz} = 2 \text{ garnet} + 2 \text{ sapphirine}_{(7:9:3)} + 2 \text{ sillimanite} \quad (15)$$

In Figure 10a two continuous Fe^{2+}–Mg reactions would occur in the three-phase fields garnet–sapphirine–spinel and garnet–sapphirine–quartz, which are, respectively:

$$\text{garnet} + 32 \text{ spinel} + 12 \text{ sillimanite} = 10 \text{ sapphirine}_{(7:9:3)} \quad (16)$$

$$6 \text{ sapphirine}_{(7:9:3)} + 32 \text{ quartz} = 7 \text{ garnet} + 20 \text{ sillimanite} \quad (17)$$

https://doi.org/10.1017/S0016756814000399 Published online by Cambridge University Press

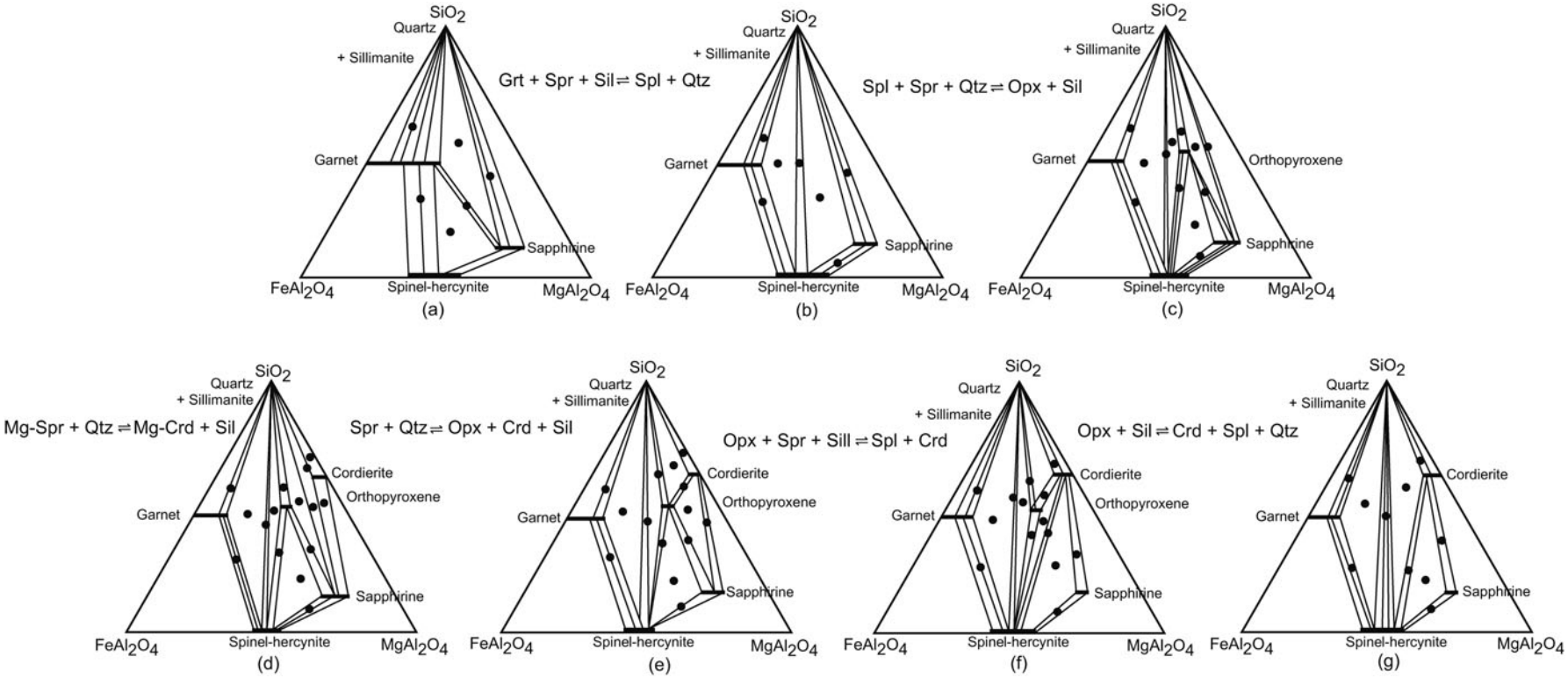

Figure 10. Phase compatibility relationships from the sapphirine–spinel granulites shown in the projection from sillimanite on to the SiO_2–$FeAl_2O_4$–$MgAl_2O_4$ plane of the FeO–MgO–Al_2O_3–SiO_2 tetrahedron; sequence of reactions is deduced from the coronas and other reaction textures and phase compatibility relationships of the mineral phases (a–g). Filled circles show the two- and three-phase assemblages observed.

Sapphirine rims around spinel, separating spinel from two other reactants garnet + sillimanite and sapphirine rimmed by garnet + sillimanite in a matrix of quartz as observed in sample no. 1110 are textural evidence of reactions (16) and (17), respectively.

6.b. Reactions involving orthopyroxene

The spinel–sapphirine–sillimanite–orthopyroxene corona (Fig. 7b) in the matrix of quartz may be attributed to the discontinuous Fe^{2+}–Mg reaction:

$$\text{sapphirine}_{(2:2:1)} + 2 \text{ spinel} + 10 \text{ quartz} = 3 \text{ orthopyroxene} + 6 \text{ sillimanite} \quad (18)$$

The reaction is evident from the formation of orthopyroxene–spinel, orthopyroxene–sapphirine and orthopyroxene–quartz joins within the three-phase field of spinel–sapphirine–quartz in the sillimanite projection (Fig. 10b, c).

In the sillimanite projection shown in Figure 10c, three continuous Fe^{+2}–Mg reactions, which may occur in the three-phase fields of sapphirine–orthopyroxene–quartz, spinel–orthopyroxene–quartz and sapphirine–cordierite–quartz, respectively, are as follows:

$$4 \text{ sapphirine}_{(7:9:3)} + 26 \text{ quartz} = 7 \text{ orthopyroxene} + 18 \text{ sillimanite} \quad (19)$$

$$2 \text{ spinel} + 4 \text{ quartz} = \text{orthopyroxene} + 2 \text{ sillimanite} \quad (20)$$

$$4 \text{ sapphirine}_{(7:9:3)} + 33 \text{ quartz} = 7 \text{ cordierite} + 4 \text{ sillimanite} \quad (21)$$

Coronas of sapphirine–sillimanite–orthopyroxene, spinel sillimanite–orthopyroxene and sapphirine–sillimanite–cordierite can be explained by the reactions (19), (20) and (21), respectively.

Inclusions of spinel within garnet and sillimanite indicate the reaction:

$$3 \text{ spinel} + 5 \text{ quartz} = \text{garnet} + 2 \text{ sillimanite} \quad (22)$$

within the three-phase field of garnet–spinel–quartz (Fig. 10b, c). At a later stage sapphirine became incompatible with quartz, presumably due to the discontinuous Fe^{2+}–Mg reaction

$$8 \text{ sapphirine}_{(7:9:3)} + 59 \text{ quartz} = 7 \text{ orthopyroxene} + 7 \text{ cordierite} + 22 \text{ sillimanite} \quad (23)$$

which may explain the corona of sapphirine–sillimanite–cordierite–orthopyroxene. The corona spinel–sillimanite–cordierite–orthopyroxene may be attributed to two continuous Fe^{2+}–Mg reactions:

$$2 \text{ spinel} + 4 \text{ quartz} = \text{orthopyroxene} + 2 \text{ sillimanite} \quad (24)$$

and

$$\text{orthopyroxene} + 2 \text{ sillimanite} + \text{quartz} = \text{cordierite} \quad (25)$$

In the sillimanite projections (Fig. 10e), the sapphirine–quartz tie line is intersected by the cordierite–orthopyroxene tie line. This reaction is evident from the diagram $(MgO + FeO)$–$(Al_2O_3 + Fe_2O_3 + Cr_2O_3)$–$SiO_2$ (Fig. 9), in which the composition of cordierite plots on the spinel–quartz tie line.

In the sillimanite projection the Reaction (25) suggests that the *P*–*T* trajectory crossed over the two reactions:

$$16 \text{ sapphirine}_{(7:9:3)} + 33 \text{ orthopyroxene} + 50 \text{ sillimanite} = 66 \text{ spinel} + 28 \text{ cordierite} \quad (26)$$

$$3 \text{ orthopyroxene} + 6 \text{ sillimanite} = 2 \text{ spinel} + 2 \text{ cordierite} + 2 \text{ quartz} \quad (27)$$

The presence of coarse-grained porphyroblasts of cordierite in contact with orthopyroxene, in a zone depleted in quartz or sillimanite, can be explained by the continuous Fe^{2+}–Mg Reaction (25).

6.c. Possible reactions involving osumilite

Osumilite was most likely stable during the early stage of metamorphism of sapphirine–spinel-bearing granulite but has been replaced by symplectite containing cordierite–orthopyroxene–K-feldspar–quartz after the thermal peak of metamorphism. The presence of inclusions of coarse prisms of orthopyroxene and sapphirine within cordierite–orthopyroxene–K-feldspar–quartz osumilite symplectites suggests osumilite formation by the prograde continuous Fe^{2+}–Mg reaction

$$4 \text{ sapphirine}_{(7:9:3)} + 2 \text{ orthopyroxene} + 9 \text{ K - feldspar} + 53 \text{ quartz} = 9 \text{ osumilite} \quad (28)$$

Sapphirine rimmed by sillimanite and/or cordierite within the symplectite may be attributed to the reactions:

$$\text{sapphirine} + \text{sillimanite} + \text{osumilite} = \text{cordierite} + \text{K - feldspar} + \text{quartz} \quad (29)$$

$$2 \text{ sapphirine} + \text{osumilite} + 14 \text{ quartz} = 5 \text{ cordierite} + \text{sanidine} \quad (30)$$

The common presence of cordierite + orthopyroxene + K-feldspar + quartz and sillimanite + orthopyroxene + K-feldspar + quartz symplectites in the sapphirine–spinel-bearing granulite are, respectively, related to the breakdown of osumilite due to the continuous Fe^{+2}–Mg reactions (29) and (30).

Retrograde phlogopite replacing the symplectite of cordierite–orthopyroxene–K-feldspar–quartz formed from the breakdown of osumilite may be related to the reaction

$$\text{orthopyroxene} + \text{cordierite} + \text{K - feldspar} + H_2O = \text{phlogopite} + \text{quartz} \quad (31)$$

https://doi.org/10.1017/S0016756814000399 Published online by Cambridge University Press

6.d. Oxidation reactions

The presence of ilmenite–haematite intergrowth within spinel in the spinel–sillimanite–orthopyroxene coronas and elevated Fe^{3+} contents of sapphirine, spinel and sillimanite suggest oxidizing conditions during the formation of these coronas.

In the sapphirine–spinel-bearing rocks spinel is separated from quartz presumably by a discontinuous Fe–Mg–Ti reaction:

$$\text{spinel} + \text{rutile} + \text{quartz} = \text{ilmo - hematite} + \text{sillimanite} + \text{orthopyroxene} + O_2 \quad (32)$$

In some reaction coronas spinel–haemo-ilmenite ± corundum is rimmed by sillimanite. This may be attributed to the reactions

$$\text{spinel}_{ss(1)} + \text{rutile} + O_2 = \text{spinel}_{ss(2)} + \text{hemo - ilmenite} + \text{corundum} \quad (33)$$

and

$$\text{spinel}_{ss(1)} + \text{rutile} + \text{quartz} + O_2 = \text{spinel}_{ss(2)} + \text{hemo - ilmenite} + \text{sillimanite} \quad (34)$$

$\text{Spinel}_{ss(1)}$ has a higher Fe^{+2}/Mg ratio than $\text{spinel}_{ss(2)}$.

Rutile is acting as a reactant in these reactions, which is evident from its occurrence along with spinel in the core of the coronas in relatively less oxidized rocks. The corona types (Fig. 7a) related to reactions (33) and (34) are: (spinel–haemo-ilmenite ± corundum)–sillimanite–orthopyroxene, (spinel–haemo-ilmenite)–sillimanite–orthopyroxene and (spinel–haemo-ilmenite)–sapphirine–sillimanite–orthopyroxene.

7. Petrogenetic grids

At low fO_2, the [Spl]-, [Qtz]-, [Opx]- and [Sil]-absent invariant points are stable, whereas the [Crd]-, [Grt]- and [Spr]-absent invariant points are metastable. A particular invariant point stable at low fO_2 becomes metastable at high fO_2 as the topology of the diagram is inverted and a number of univariant and divariant mineral equilibria are restricted in their occurrence to either low or high fO_2, respectively. Analytical data on sapphirine, spinel, garnet, orthopyroxene and sillimanite indicate that these phases may contain significant amounts of Fe^{3+} and, therefore, crystallized at relatively high fO_2.

The association of spinel–sapphirine–quartz with garnet and sillimanite and the corona type spinel–sapphirine–(garnet–sillimanite) in a matrix of quartz are related to the (Opx)-absent univariant Fe–Mg reaction (Fig. 11) emerging from the [Crd] invariant point, which is compatible in the FMAS grids for high fO_2 proposed by Hensen (1986). Similarly, the association of spinel–sapphirine–quartz with orthopyroxene–sillimanite and the corona type spinel–sapphirine–sillimanite, spinel–sillimanite–orthopyroxene and sapphirine–sillimanite–orthopyroxene are related to the univariant reaction (Fig. 11) emerging from the [Crd]- and [Grt]-absent invariant points. The coronas sapphirine–sillimanite–cordierite–orthopyroxene and sapphirine–sillimanite–cordierite in a matrix of quartz are related to the (Spl)-absent reaction (Fig. 11) from the [Grt]-absent invariant point.

Furthermore, the corona of spinel–sillimanite–cordierite–orthopyroxene can be explained by combination of the reactions (23) and (24). Similarly the corona rim of cordierite between spinel and quartz is due to Reaction (13). These reactions are related to the univariant Reaction (26) from (Grt)- and (Spr)-absent reactions.

Thus, it is evident that the [Crd]-, [Grt]- and [Spr]-absent invariant points are stable in the sapphirine–spinel-bearing rocks of the study area. Therefore, the petrogenetic grid in the FMAS system for high fO_2 (Fig. 11), as proposed by Hensen (1986), is applicable to these rocks.

The sequence of development of coronas and other reaction textures is shown in the petrogenetic grid in the FMASH system after Hensen (1986) at high fO_2 (Fig. 11). The earlier recognizable stage in the mineral history using the above petrogenetic grid is represented on the high-pressure side by orthopyroxene or garnet with Mg-rich cores coexisting with sillimanite. The spinel–quartz and sapphirine–quartz grain contacts indicate that these minerals coexisted during the thermal peak of metamorphism. The development of reaction textures, especially polymineralic coronas including coronas of spinel–sapphirine–(garnet + sillimanite), spinel–sapphirine–sillimanite–orthopyroxene and spinel–sillimanite–cordierite–orthopyroxene in a matrix of quartz, as well as rims of cordierite between spinel and quartz, demonstrate decreasing *P–T* conditions during the dynamic uplift history. The sequence of the development of reaction coronas also confirms a retrograde path passing through the [Crd]-absent invariant point to (Spl)-absent univariant reaction from [Grt], to the univariant reaction from the [Spr]- and [Grt]-absent invariant points (Fig. 11). Despite errors inherent in the calculations, the texturally defined subassemblages in the sapphirine–spinel-bearing granulite yield distinct *P–T* conditions for the various evolutionary stages. The *P–T* estimates calculated through the application of THERMOCALC (version 3.21; Holland & Powell, 1998) indicate decreasing *P–T* combinations of about 10.5 kbar/1000 °C, 9 kbar/900 °C and 5 kbar/800 °C, the latter two conforming to the [Cdr]- and [Spr]-absent invariant points, respectively.

8. *P–T* pseudosection modelling for sapphirine-bearing granulite

Based on the dominant minerals and their chemical compositions, the phase equilibria of the Diguva Sonaba granulites from the EGMB can be modelled in the system Na_2O–CaO–K_2O–FeO–MgO–Al_2O_3–SiO_2–TiO_2–H_2O (NCKFMASTH). A *P–T* pseudosection for the sapphirine-bearing granulite (sample no.

https://doi.org/10.1017/S0016756814000399 Published online by Cambridge University Press

Table 1. Solution notation, formulae and model sources for phase diagram calculation

Symbol	Solution	Formula	Source
Bt	Biotite	$K[Mg_xFe_yMn_{1-x-y}]_{3-u-v-w}Fe^{3+}{}_wTi_uAl_{1+v}Si_{3-v}O_{10}(OH)_{2-2u}$, $x+y\_1$, $u+v+w\_1$	Tajcmanová *et al.* (2009)
Grt	Garnet	$Fe_{3x}Ca_{3y}Mg_{3z}Mn_{3(1-x-y-z)}Al_2Si_3O_{12}$.$x+y+z\_1$	Holland & Powell (1998)
Opx	Orthopyroxene	$[Mg_xFe_{1-x}]_{2-y}Al_{2y}Si_{2-y}O_6$	Holland & Powell (1996)
Crd	Cordierite	$Mg_{2x}Fe_{2y}Mn_2(1-x-y)Al_4Si_5O_{18}\bullet(H2O)_z$, $x+y\_1$	Ideal
Spl	Spinel	$Mg_xFe_{1-x}Al_2O_3$	Holland & Powell (1996)
Spr	Sapphirine	$[Mg_xFe_{1-x}]_{4-y/2}Al_{9-y}Si_{2-y/2}O_{20}$	Holland & Powell (1996)
Pl, Kfs	Feldspar	$K_yNa_xCa_{1-x-y}Al_{2-x-y}Si_{2+x+y}O_8$.$x+y\_1$	Benisek *et al.* (2010)
Liq	Melt	Na–Mg–Al–Si–K–Ca–Fe hydrous silicate melt	Holland & Powell (2001); White *et al.* (2001)

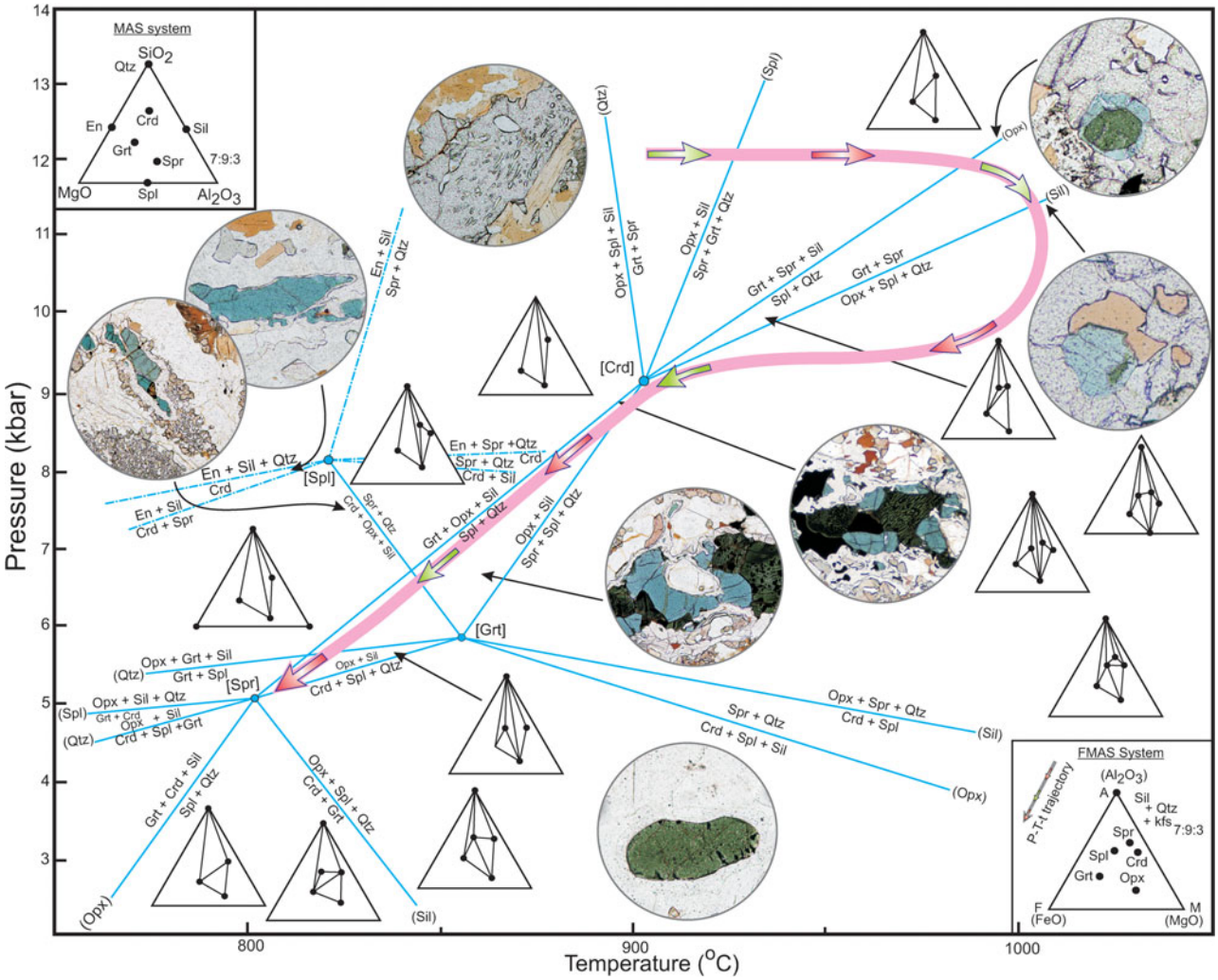

Figure 11. (Colour online) *P–T* petrogenetic grid in the FeO–MgO–Al_2O_3–SiO_2 (FMAS) system at high fO_2 after Hensen (1986). The mineral assemblages in the divarient fields are shown by AFM projection. Minerals in parentheses represent univariant reactions diverging from the invariant points, indicated by square brackets. The sequence of development of coronas and other reaction textures suggest a retrograde path passing through the [Crd]-absent invariant point and along the (Spr)-absent univariant reaction towards the [Spr]-absent invariant point. The presence of orthopyroxene coexisting with sillimanite in many samples of sapphirine–spinel-bearing rocks in the area suggests a prograde path passing from the low- to the high-temperature side of the (Spl)-absent univariant curve. Thus the *P–T* trajectory appears to have been clockwise with nearly isothermal, presumably rapid decompression during the metamorphic evolution.

1111) was calculated using the software Perple_X 6.66 (Connolly, 2005) (Fig. 12). Solution models used in the calculations are given in Table 1. Comparing the textural observations with the calculated pseudosection, the *P–T* path associated with the series of changes that occurred in the rock is inferred. In sample no. 1111, the prograde assemblage Bt–Opx–Grt–Pl–Ky is quadravariant (v = 4) in NCKFMASTH and its conversion to the assemblage Opx–Grt–Pl–Sil suggests biotite dehydration. The peak assemblage Grt–Opx–Sil–Pl is stable between 11 and 12 kbar at temperatures above 1000 °C. High Al contents (0.19) in coarse-grained

https://doi.org/10.1017/S0016756814000399 Published online by Cambridge University Press

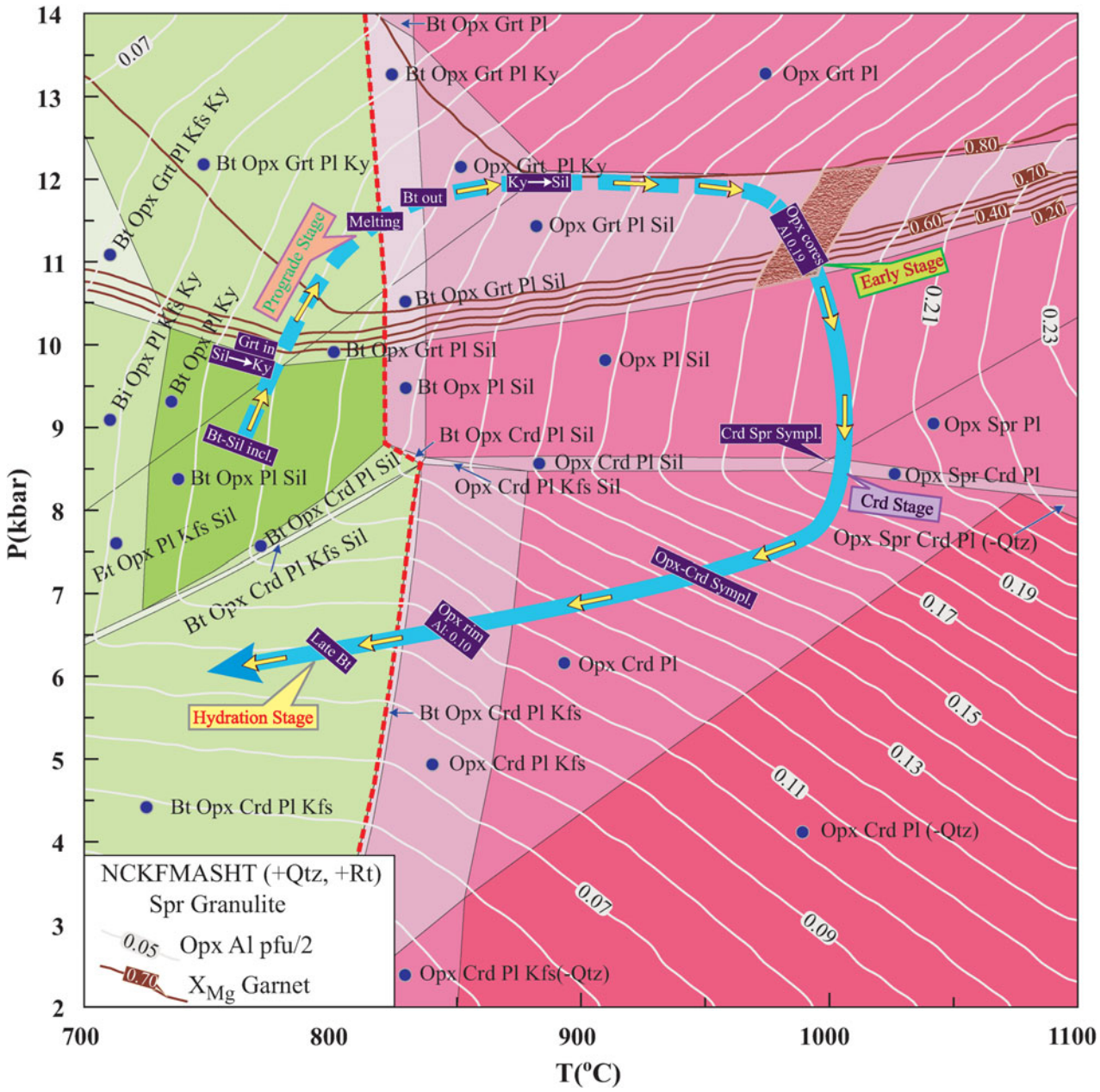

Figure 12. (Colour online) Calculated *P–T* pseudosections for sapphirine-bearing granulite without spinel (sample no. 1111) in the system NCKFMASHT (+ Qtz + Rt + Liq (above solidus)). Bulk composition in mole % (Na_2O 2.50, CaO 1.39, K_2O 1.23, FeO 3.69, MgO 19.24, Al_2O_3 10.83, SiO_2 59.03, H_2O 1.76, TiO_2 0.31). The solidus (for a_{H2O} = 0.02) is marked by the dashed line. The pseudosection is contoured for the isopleths of (a) X_{Mg}(Grt) and (b) X_{Al}(Opx). The stippled areas mark peak metamorphic *P–T* ranges inferred from mineral compositional data. Prograde and retrograde paths are marked by dashed and continuous lines, respectively.

orthopyroxene indicate temperatures of *c*. 1000 °C. A *P–T* path may be drawn on the basis of calculated isopleths and measured mineral chemistry obtained by EPMA. As seen in Figure 12, garnet is stable above 10 kbar and contoured isopleths of X_{Mg} for the garnet have flat slopes. Symplectitic intergrowths provide evidence for decompression. For instance, the formation of different coronas indicates entry into the Opx–Pl–Sil/Spr fields with decreasing pressure, whereas the subsequent formation of cordierite at lower pressure led to Crd–Spr/Opx symplectites. Decrease in Al content in orthopyroxene (0.15–0.07) and formation of retrograde biotite reflect continued cooling below the solidus at temperature less than 800 °C (hydration stage).

9. Discussion

The FMAS grid for high fO_2 (after Hensen, 1986) provides a useful framework to constrain semiquantitatively the *P–T* history of sapphirine-bearing granulites (Fig. 11):

(i) A *clockwise P–T path* is indicated by the presence of prograde mineral relics and textural evidence for the presence of sillimanite pseudomorphs after kyanite blades (Fig. 13p).

https://doi.org/10.1017/S0016756814000399 Published online by Cambridge University Press

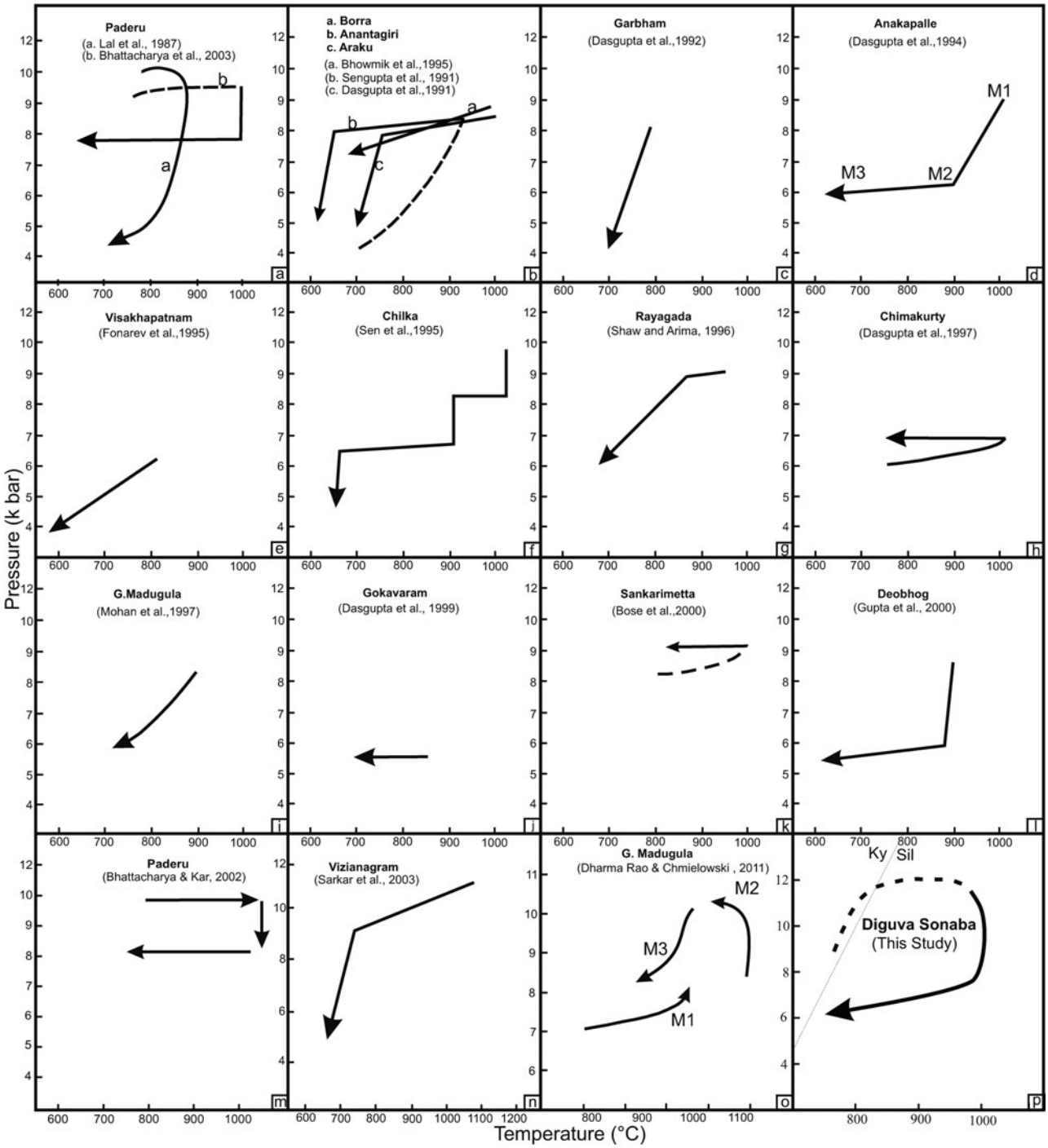

Figure 13. (a–p) *P–T* paths suggested by various workers for the granulites in different areas of the EGMB.

(ii) During the *thermal peak of metamorphism*, sapphirine + quartz and spinel + quartz were stable at *P–T* conditions of 10–12 kbar and > 950 °C. Garnet porphyroblasts, orthopyroxene prisms, blocky sillimanite and corroded biotite are interpreted as part of the primary parageneses. Moreover, abundant symplectitic intergrowths of cordierite + quartz + K-feldspar + orthopyroxene are interpreted as breakdown products of peak-metamorphic osumilite.

(iii) During the subsequent corona formation stage, sapphirine and spinel were isolated from quartz by several spectacular corona-forming reactions that indicate *isobaric cooling*. The retrograde *P–T* path passes through the (Opx)- and (Grt)-absent reactions around the [Crd]-absent invariant point.

(iv) Subsequent development of cordierite is due to *decompression* and indicates a *P–T* path passing through (Grt, Spl) from the [Spr]-absent invariant point of the *P–T* grid for the FMAS system at high fO_2.

(v) During a *late stage* and decreasing *P–T* conditions, biotite, biotite–quartz intergrowths, biotite symplectites and fibrolite matted with biotite replaced earlier grown garnet porphyroblasts, orthopyroxene prisms, cordierite and K-feldspar.

https://doi.org/10.1017/S0016756814000399 Published online by Cambridge University Press

The decompressional *P–T* trajectory may be ascribed to a geotectonic setting dominated by exhumation after crustal thickening. The exhumation mechanism, however, remains uncertain. Tectonic models for granulite formation, which take into account a decompressive *P–T* path, include (i) crustal thickening due to collisional models (Thompson & England, 1984) and (ii) an extensional regime involving a crust of near-normal thickness (Sandiford & Powell, 1986). Calculated peak *P–T* conditions suggest that the Diguva Sonaba sapphirine-spinel-bearing granulites were buried to depths of *c*. 42 km. The crustal thickness beneath the EGMB is now *c*. 35 km (Kumar *et al.* 2004), indicating that the total crustal thickness may have been as much as *c*. 77 km. Such a crustal thickness could be possibly generated by collision tectonics. Clockwise and anticlockwise paths may be distinguished on the basis of the geometry of the prograde path and not on that of the retrograde path. However, for most of the EGMB, the prograde *P–T* trajectory is not well documented (Fig. 13). The EGMB has been the subject of numerous petrological studies involving sapphirine-bearing granulite, all of which describe a great variety of different, in places contradictory, *P–T* paths (Fig. 13). A *P–T* path involving initial isobaric cooling followed by isothermal decompression has been advocated by several workers in the EGMB (Kamineni & Rao, 1988; Sengupta *et al.* 1990; Dasgupta *et al.* 1995; Rao *et al.* 1995; Shaw & Arima, 1998; Dharma Rao, Santosh & Chmielowski, 2012) but in the absence of well-constrained *P–T* histories ambiguity remains concerning clockwise and anticlockwise *P–T* paths. Recently, Korhonen *et al.* (2011, 2013) suggested that the EGMB records a single long-lived high-grade metamorphic evolution and the U–Pb zircon age populations between *c*. 1130 Ma and *c*. 930 Ma correspond to a single prograde and retrograde metamorphic evolution. Discrimination between these tectonic models is also hindered mainly by a lack of data on the cooling history and inadequate systematic isotopic age data in the EGMB. In the present study, the overall textural evidence, as well as semiquantitative petrogenetic grid and pseudosection approach point to a clockwise UHT *P–T* path in the Diguva Sonaba granulites, which is marked by post-peak isothermal decompression (Fig. 13p).

10. Conclusions

The Diguva Sonaba area is part of the multiply deformed granulite-facies terrain of the EGMB, India. A prograde *P–T* path has been inferred for the mineral assemblages in the Diguva Sonaba granulites. An early stage during the thermal peak is recognized by the coexistence of sapphirine + quartz, and spinel + quartz in textural equilibrium. Garnet, orthopyroxene, sillimanite, biotite and possibly osumilite are interpreted as part of the peak metamorphic parageneses. This was followed by several cordierite-forming reactions related to decompression. During the subsequent corona formation stage, sapphirine and spinel became isolated from quartz by several spectacular coronas that can be explained by nearly isobaric cooling. During a late stage, biotite, garnet–quartz intergrowths, biotite–quartz symplectite and fibrolite matted with biotite replaced earlier garnet porphyroblasts, orthopyroxene, cordierite and K-feldspar during retrograde overprint. Reaction textures, petrogenetic grid and *P–T* pseudosection constraints suggest extreme *P–T* conditions of 10–12 kbar and > 950 °C and a high-temperature decompression path for the sapphirine–spinel-bearing granulites. Based on prograde and retrograde mineral assemblages as well as a sequence of isopleths, a clockwise metamorphic *P–T* trajectory could be defined.

Acknowledgements. Discussions with, and numerous helpful suggestions by, Professor R. K. Lal are deeply appreciated. The authors acknowledge the detailed technical advice given by J. A. D. Connolly on the use of the Perple_X software. The manuscript benefitted from constructive reviews by M. Okrusch and the editor. This work was financially supported by the Ministry of Earth Sciences, (MoES) New Delhi, under the research project (P-07-578), and by the DFG (Deutsche Forschungsgemeinschaft; grant No. Fr 2183/7–1).

Supplementary material

To view supplementary material for this article, please visit http://dx.doi.org/10.1017/S0016756814000399.

References

ACKERMAND, D., HERD, R. K., REINHANDT, M. & WNDLEY, B. F. 1987. Sapphirine paragenesis from the Caraiba Complex, Bahia, Brazil. The influence of Fe^{2+}-Fe^{3+} distribution on the stability of sapphirine in natural assemblages. *Journal of Metamorphic Geology* **5**, 323–39.

ADJERID, Z., GODARD, G., OUZEGANES, K. H. & KIENAST, J. R. 2013. Multistage progressive evolution of rare osumilite-bearing assemblages preserved in ultrahigh-temperature granulites from In Ouzzal (Hoggar, Algeria). *Journal of Metamorphic Geology* **31**, 505–24.

AFTALION, M., BOWES, D. R., DASH, B. & FALLICK, A. E. 2000. Late Pan-African thermal history in Eastern Ghats terrane, India, from U-Pb and K-Ar isotopic study of the Mid-Proterozoic Khariar alkali syenite, Orissa. *Geological Survey of India Special Publication* **57**, 26–33.

BENISEK, A., DACHS, E. & KROLL, H. 2010. A ternary feldspar-mixing model based on calorimetric data: development and application. *Contributions to Mineralogy and Petrology* **160**, 327–37.

BERG, J. H. & WHEELER, II, E. P. 1976. Osumilite of deep-seated origin in contact aureole of the anorthositic Nain complex, Labrador, Canada. *American Mineralogist* **61**, 29–37.

BHATTACHARYA, S. & KAR, R. 2002. High-temperature dehydration melting and decompressive P-T path in a granulite complex from the Eastern Ghats, India. *Contributions to Mineralogy and Petrology* **143**, 175–91.

BHATTACHARYA, S., KAR, R., TEIXEIRA, W. & BASEI, M. 2003. High-temperature crustal anatexis in a clockwise P-T-t path: isotopic evidence from a granulite-granitoid suite in the Eastern Ghats belt, India. *Journal of the Geological Society, London* **160**, 39–46.

BHOWMIK, S. K., DASGUPTA, S., HOERNES, S. & BHATTACHARYA, P. K. 1995. Extremely high

temperature calcareous granulites from the Eastern Ghats, India: evidence for isobaric cooling, fluid buffering, and terminal channelized fluid flow. *European Journal of Mineralogy* **7**, 689–703.

BOSE, S. & DAS, K. 2007. Sapphirine + quartz assemblage in contrasting textural modes from the Eastern Ghats Belt, India: implications for stability relations in UHT metamorphism and retrograde processes. *Gondwana Research* **11**, 492–503.

BOSE, S., DAS, K., DASGUPTA, S., MIURA, H. & FUKUOKA, M. 2006. Exsolution textures in orthopyroxene in aluminous granulites as indicators of UHT metamorphism: new evidence from the Eastern Ghats Belt, India. *Lithos* **92**, 506–23.

BOSE, S., DUNKLEY, D. J., DASGUPTA, S., DAS, K. & ARIMA, M. 2011. India-Antarctica-Australia-Laurentia connection in the Paleoproterozoic–Mesoproterozoic revisited: evidence from new zircon U-Pb and monazite chemical age data from the Eastern Ghats Belt, India. *Geological Society of America Bulletin* **123**, 2031–49.

BOSE, S., FUKUOKA, M., SENGUPTA, P. & DASGUPTA, S. 2000. Evolution of high Mg-Al granulites from Sunkarametta, Eastern Ghats, India: evidence for a lower crustal heating-cooling trajectory. *Journal of Metamorphic Geology* **18**, 223–40.

BRANDT, S., SCHENK, V., RAITH, M. M., APPEL, P., GERDES, A. & SRIKANTAPPA, C. 2011. Late-Neoproterozoic clockwise P-T evolution of sapphirine-bearing HP-UHT granulites from the Palni Hills (South India): new constraints from phase diagram modelling and LA-ICP-MS zircon dating combined with in-situ EMP monazite dating. *Journal of Petrology* **52**, 1813–56.

CHATTERJEE, N. D. & SCHREYER, W. 1972. The reaction enstatite$_{ss}$ + sillimanite = sapphirine$_{ss}$ + quartz in the system MgO–Al_2O_3–SiO_2. *Contributions to Mineralogy and Petrology* **36**, 49–62.

CONDIE, K. C. 2005. *Earth as an Evolving Planetary System*. Burlington, Vermont: Elsevier, 447 pp.

CONNOLLY, J. A. D. 2005. Computation of phase equilibria by linear programming: a tool for geodynamic modeling and its application to subduction zone decarbonation. *Earth Planetary Science Letters* **236**, 524–41.

DAS, K., BOSE, S., KARMAKAR, S., DUNKLEY, D. J. & DASGUPTA, S. 2011. Multiple tectonometamorphic imprints in the lower crust: first evidence of ca. 950 Ma (zircon U-Pb SHRIMP) compressional reworking of UHT aluminous granulites from the Eastern Ghats Belt, India. *Geological Journal* **46**, 217–39.

DASGUPTA, S., BOSE, S. & DAS, K. 2013. Tectonic evolution of the Eastern Ghats Belt, India. *Precambrian Research* **227**, 247–58.

DASGUPTA, S., EHL, J., RAITH, M. M. & SENGUPTA, P. 1997. Mid-crustal contact metamorphism around the Chimakurthy mafic-ultramafic complex, Eastern Ghats Belt, India. *Contributions to Mineralogy and Petrology* **129**, 182–97.

DASGUPTA, S., RAITH, M. & SARKAR, S. 2008. New perspective in the study of the Precambrian continental crust of India: an integrated sedimentologic, isotopic, tectonometamorphic and seismological appraisal. *Precambrian Research* **162**, 1–316.

DASGUPTA, S., SANYAL, S., SENGUPTA, P. & FUKUOKA, M. 1994. Petrology of the granulites from Anakapalle – evidence for Proterozoic decompression in the Eastern Ghats, India. *Journal of Petrology* **35**, 433–59.

DASGUPTA, S. & SENGUPTA, P. 2003. Indo-Antarctic correlation: a perspective from the Eastern Ghats Granulite Belt, India. In *Proterozoic East Gondwana: Supercontinent Assembly and Breakup* (eds M. Yoshida, B. F. Windley & S. Dasgupta), pp. 131–43. Geological Society of London, Special Publication no. 206.

DASGUPTA, S., SENGUPTA, P., EHL, J., RAITH, M. & BARDHAN, S. 1995. Reaction textures in a suite of spinel granulites from the Eastern Ghats Belt, India: evidence for polymetamorphism, a partial petrogenetic grid in the system KFMASH and roles of ZnO and Fe_2O_3. *Journal of Petrology* **36**, 435–61.

DASGUPTA, S., SENGUPTA, S., FUKUOKA, M. & CHAKRABORTI, S. 1992. Dehydration melting, fluid buffering and decompressional P–T path in a granulite complex from the Eastern Ghats, India. *Journal of Metamorphic Geology* **10**, 777–88.

DASGUPTA, S., SENGUPTA, P., GUHA, D. & FUKUOKA, M. 1991. A refined garnet–biotite Fe–Mg exchange geothermometer and its application in amphibolites and granulites. *Contributions to Mineralogy and Petrology* **109**, 130–7.

DASGUPTA, S., SENGUPTA, P., MONDAL, A. & FUKUOKA, M. 1993. Mineral chemistry and reaction textures in metabasites from the Eastern Ghats belt, India and their implications. *Mineralogical Magazine* **57**, 113–20.

DASGUPTA, S., SENGUPTA, P., SENGUPTA, P. R., EHL, J. & RAITTH, M. 1999. Petrology of gedrite-bearing rocks in mid-crustal ductile shear zones from the Eastern Ghats Belt, India. *Journal of Metamorphic Geology* **17**, 765–78.

DHARMA RAO, C. V. & CHMIELOWSKI, R. 2011. New constraints on the metamorphic evolution of the Eastern Ghats Belt, India: based on relict composite inclusions in garnet from ultra high-temperature sapphirine granulites. *Geological Journal* **46**, 240–62.

DHARMA RAO, C. V., SANTOSH, M. & CHMIELOWSKI, R. M. 2012. Sapphirine granulites from Panasapattu, Eastern Ghats belt, India: ultrahigh-temperature metamorphism in a Proterozoic convergent plate margin. *Geoscience Frontiers* **3**, 9–31.

ELLIS, D. J. 1980. Osumilite-sapphirine-quartz granulites from Enderby land, Antarctica. P-T conditions of metamorphism, implications for garnet-cordierite equilibria and the evolution of deep crust. *Contributions to Mineralogy and Petrology* **74**, 201–10.

FONAREV, V. I., RAO, A. T. & KONILOVE, A. N. 1995. Evaluation of pressure-temperature of metamorphism and tectonothermal history of granulites from the Visakhapatnam area in the Eastern Ghats, India. In *India and Antarctica During the Precambrian* (eds M. Yoshida & M. Santosh), pp. 111–24. Memoir of the Geological Society of India no. 34.

GREW, E. S. 1982. Sapphirine, kornerupine and sillimanite + orthopyroxene in the charnockite region of south India. *Journal of Petrology* **21**, 39–68.

GUPTA, S., BHATTACHARYA, A., RAITH, M. & NANDA, J. K. 2000. Contrasting pressure–temperature-deformation history across a vestigial craton-mobile belt boundary: the western margin of the Eastern Ghats belt at Deobhog, India. *Journal of Metamorphic Geology* **18**, 683–97.

HENSEN, B. J. 1986. Theoretical phase relations involving cordierite and garnet revisited: the influence of oxygen fugacity on the stability of sapphirine and spinel in the system Mg-Fe-Al-Si-O. *Contributions to Mineralogy and Petrology* **92**, 362–7.

HENSEN, B. J. & GREEN, D. H. 1971. Experimental study of cordierite and garnet in pelitic compositions at high pressures and temperatures I. Composition with excess alumino-silicate. *Contributions to Mineralogy and Petrology* **35**, 331–54.

HOLLAND, T. J. B. & POWELL, R. 1996. Thermodynamics of order-disorder in minerals. 2. Symmetric formalism applied to solid solutions. *American Mineralogist* **81**, 1425–37.

HOLLAND, T. J. B. & POWELL, R. 1998. An internally consistent thermodynamic data set for phases of petrological interest. *Journal of Metamorphic Geology* **16**, 309–43.

HOLLAND, T. J. B. & POWELL, R. 2001. Calculation of phase relations involving haplogranitic melts using an internally consistent thermodynamic dataset. *Journal of Petrology* **42**, 673–83.

HÖRMANN, P. K., RAITH, M., RAASE, P., ACKERMAND, D. & SEIFERT, F. 1980. The granulite complex of Finnish Lapland: petrology and metamorphic condition in the Ivalojokii-Inarijarvi, area. *Bulletin of the Geological Survey of Finland* **308**, 1–95.

KAMINENI, D. C & RAO, A. T. 1988. Sapphirine granulites from the Kakanuru area, Eastern Ghats, India. *American Mineralogist* **73**, 692–700.

KORHONEN, F. J., CLARK, C., BROWN, M., BHATTACHARYA, S. & TAYLOR, R. 2013. How long-lived is ultrahigh temperature (UHT) metamorphism? Constraints from zircon and monazite geochronology in the Eastern Ghats orogenic belt, India. *Precambrian Research* **234**, 322–50.

KORHONEN, F. J., SAW, A. K., CLARK, C., BROWN, M. & BHATTACHARYA, S. 2011. New constraints on UHT metamorphism in the Eastern Ghats Province through the application of phase equilibria modelling and in situ geochronology. *Gondwana Research* **20**, 764–81.

KRETZ, R. 1983. Symbols for rock-forming minerals. *American Mineralogist* **68**, 277–9.

KUMAR, N., SINGH, A. P., GUPTA, S. B. & MISHRA, D. C. 2004. Gravity signature, crustal architecture and collision tectonics of the Eastern Ghats Mobile Belt. *Journal of Indian Geophysical Union* **8**, 97–106.

LAL, R. K. 2003. Metamorphic evolution of granulites from southern Indian Shield. In *Milestones in Petrology and Future Perspectives* (ed. A. Mohan), pp. 61–108. Memoir of the Geological Society of India no. 52.

LAL, R. K., ACKERMAND, D., RAITH, M., RAASE, P. & SEIFERT, F. 1984. Sapphirine-bearing assemblages from Kiranur, southern India: a study of chemographic relationships in the Na_2O–FeO–MgO–Al_2O_3–SiO_2–H_2O system. *Neues Jahrbuch für Mineralogie – Abhandlungen* **150**, 121–52.

LAL, R. K., ACKERMAND, D. & UPADHYAY, H. 1987. P-T-X relationships deduced from corona textures in sapphirine-spinel-quartz assemblages from Paderu, southern India. *Journal of Petrology* **28**, 1139–68.

LONKER, S. W. 1981. The P-T-X relations of the cordierite-garnet-sillimanite-quartz equilibria. *American Journal of Science* **281**, 1056–90.

MEZGER, K. & COSCA, M. A. 1999. The thermal history of the Eastern Ghats Belt (India), as revealed by U-Pb and 40Ar/39Ar dating of metamorphic and magmatic minerals: implications for the SWEAT correlation. *Precambrian Research* **94**, 251–71.

MOHAN, A., SINGH, P. K. & SACHAN, H. K. 2003. High-density carbonic fluid inclusions in charnockites from Eastern Ghats, India: petrologic implications. *Journal of Asian Earth Science* **22**, 101–13.

MOHAN, A., TRIPATHI, P. & MOTOYASHI, Y. 1997. Reaction history of sapphirine granulites and a decompressional P-T path in a granulite complex from the Eastern Ghats. *Proceedings of the Indian Academy of Sciences (Earth and Planetary Sciences)* **106**, 115–30.

MUKHOPADHYAY, D. & BASAK, K. 2009. The Eastern Ghats Belt – a polycyclic granulite terrain. *Journal of the Geological Society of India* **73**, 489–518.

MUKHOPADHYAY, A. K. & BHATTACHARYA, A. 1997. Tectonothermal evolution of the gneiss complex at Salur in the Eastern Ghats granulite belt of India. *Journal of Metamorphic Geology* **15**, 719–34.

NOWICKI, T. E., FRIMMEL, H. E. & WATERS, D. J. 1995. The occurrence of osumilite in pelitic granulite of the Namaqualand Metamorphic Complex, South Africa. *South African Journal of Geology* **98**, 191–201.

PAL, S. & BOSE, S. 1997. Mineral reactions and geothermobarometry in a suite of granulite facies rocks from Paderu, Eastern Ghats granulite belt: a reappraisal of the P-T trajectory. *Proceedings of the Indian Academy of Science (Earth and Planetary Sciences)* **106**, 77–89.

PAUL, D. K., BERMAN, T. R., MENAUGHTON, N. J., FLETCHER, I. R., POTTS, P. J., RAMAKRISHNAN, M. & AUGUSTINE, P. F. 1990. Archaean Proterozoic evolution of Indian charnockites: isotopic and geochemical evidences from granulites of the Eastern Ghats Belt. *Journal of Geology* **98**, 253–63.

RAITH, M., KARMAKAR, S. & BROWN, M. 1997. Ultra-high-temperature metamorphism and multistage decompressional evolution of sapphirine granulites from the Palni Hill Ranges, south India. *Journal of Metamorphic Geology* **15**, 379–99.

RAMAKRISHNAN, M., NANDA, J. K. & AUGUSTINE, P. F. 1998. Geological evolution of the Proterozoic Eastern Ghats Mobile Belt. *Geological Survey of India Special Publication* **44**, 1–21.

RAO, A. T., KAMINENI, D. C., ARIMA, M. & YOSHIDA, M. 1995. Mineral chemistry and metamorphic P-T conditions of a new occurrence of sapphirine granulites near Madhuravada in the Eastern Ghats, India. In *India as a Fragment of East Gondwana* (eds & A. T. Rao Santosh), pp. 109–21. Gondwana Research Group Memoir 2.

RICKERS, K., MEZGER, K. & RAITH, M. M. 2001. Evolution of the continental crust in the Proterozoic Eastern Ghats Belt, India and new constraints for Rodinia reconstruction: implications from Sm−Nd, Rb−Sr and Pb−Pb isotopes. *Precambrian Research* **112**, 183–212.

RUTTER, E. H. 1997. The influence of deformation on the extraction of crustal melts: a consideration of the role of melt-assisted granular flow. In *Deformation-Enhanced Fluid Transport in the Earth's Crust and Mantle* (ed. M. B. Holness), pp. 82–110. London: Chapman & Hall.

SANDIFORD, M. & POWELL, R. 1986. Pyroxene exsolution in granulites from Fyfe Hills, Enderby Land, Antarctica: evidence for 1000 °C metamorphic temperatures in Archaean continental crust. *American Mineralogist* **7**(1), 946–54.

SARKAR, S., SANTOSH, M., DASGUPTA, S. & FUKUOKA, M. 2003. Very high density CO2 associated with ultrahigh-temperature metamorphism in the Eastern Ghats granulite belt, India. *Geology* **31**, 51–4.

SCHREYER, W. & SEIFERT, F. 1967. Metastability and an osumilite end member in the system K_2O-MgO-Al_2O_3-H_2O and its possible bearing on the rarity of natural osumilites. *Contributions to Mineralogy and Petrology* **14**, 343–58.

SCHREYER, W. & SEIFERT, F. 1969. Compatibility relations of the aluminum silicates in the systems MgO-Al_2O_3-SiO_2-H_2O and K_2O-MgO-Al_2O3-H_2O at high pressures. *American Journal of Science* **267**, 371–88.

SEN, S. K., BHATTACHARYA, S. & ACHARYA, A. 1995. A multi-stage pressure–temperature record in the Chilka Lake granulites: the epitome of the metamorphic

evolution of Eastern Ghats, India. *Journal of Metamorphic Geology* **14**, 287–98.

SENGUPTA, A. P., DASGUPTA, S., BHUI, U. K., EHL, J. & FUKOAKA, M. 1996. Magmatic evolution of mafic granulites from Anakapalle, Eastern Ghats, India: implications for tectonic setting of a Precambrian high-grade terrain. *Journal of Southeast Asian Earth Science* **14**, 185–98.

SENGUPTA, P., DASGUPTA, S., BHATTACHARYA, P. K., FUKOKA, M., CHAKRABORTI, S. & BHOWMIK, S. 1990. Petrotectonic imprints in the sapphirine granulites from Anantagiri, Eastern Ghats Mobile Belt, India. *Journal of Petrology* **31**, 971–96.

SENGUPTA, A. P., DASGUPTA, S., EHL, J. & RAITH, M. M. 1997*a*. Thermobaric evolution of a suite of Mg-Al granulites from Paderu: further evidence for a ACW P-T path in the Eastern Ghats Belt, India. *Beihefte zum European Journal of Mineralogy* **9**(1), 331 pp.

SENGUPTA, P., DASGUPTA, S., RAITH, M., BHUI, U. K. & EHL, J. 1999. Ultra-high temperature metamorphism of metapelitic granulites from Kondapalle, Eastern Ghats Belt: implications for the Indo-Antarctic correlation. *Journal of Petrology* **40**, 1065–87.

SENGUPTA, P., KARMAKAR, S., DASGUPTA, S. & FUKUOKA, M. 1991. Petrology of spinel granulites from Araku, Eastern Ghats, India, and a petrotectonic grid for sapphirine-free rocks in the system FMAS. *Journal of Metamorphic Geology* **9**, 451–9.

SENGUPTA, A. P., SANYAL, S., DASGUPTA, S., FUKOAKA, M., EHL, J. & PAL, S. 1997*b*. Controls of mineral reactions in high-grade garnet–wollastonite–scapolite bearing calc-silicate rocks: an example from Anakapalle, Eastern Ghats, India. *Journal of Metamorphic Geology* **15**, 551–64.

SHAW, R. K. & ARIMA, M. 1996. High-temperature metamorphic imprint from calc-granulites of Rayagada, Eastern Ghats, India: implications of isobaric cooling path. *Contributions to Mineralogy and Petrology* **126**,169–80.

SHAW, R. K. & ARIMA, M. 1998. A corundum-quartz assemblage from the Eastern Ghats Granulite Belt, India: evidence of high P–T metamorphism? *Journal of Metamorphic Geology* **16**, 189–96.

TAJCMANOVA, L., CONNOLLY, J. A. D. & CESARE, B. 2009. A thermodynamic model for titanium and ferric iron solution in biotite. *Journal of Metamorphic Geology* **27**, 153–64.

THOMPSON, A. B. & ENGLAND, P. C. 1984. Pressure-temperature-time paths of regional metamorphism II: their inference and interpretation using mineral assemblages in metamorphic rocks. *Journal of Petrology* **25**, 929–54.

UPADHYAY, D., GERDES, A. & RAITH, M. M. 2009. Unraveling sedimentary provenance and tectonothermal history of high to ultra-high temperature metapelites using zircon and monazite chemistry: a case study from the Eastern Ghats Belt, India. *Journal of Geology* **117**, 665–83.

UPADHYAY, D., RAITH, M. M., MEZGER, K., BHATTACHARYA, A. & KINNY, P. D. 2006. Mesoproterozoic rifting and Pan-African continental collision in South-Eastern India: evidence from the Khariar alkaline complex. *Contributions to Mineralogy and Petrology* **151**, 434–56.

VINOGRADOV, A., TUGARINOV, A., ZHYKOV, C., STAPNIKOVA, N., BIBIKOVA, E. & KORRE, K. 1964. Geochronology of the Indian Precambrian. Report of the 22nd International Geological Congress, New Delhi, vol. 10, pp. 553–67.

WHITE, R. W. & POWELL, R. & HOLLAND, T. J. B. 2001. Calculation of partial melting equilibria in the system Na_2O-CaO-K_2O-FeO-MgO-Al_2O_3-SiO_2-H_2O (NCKFMASH). *Journal of Metamorphic Geology* **19**, 139–53.

YOSHIDA, M., JACOBS, J., SANTOSH, M. & RAJESH, H. M. 2003. Role of Pan-African events in the Circum-East Antarctic Orogen of East Gondwana: a critical overview. In *Proterozoic East Gondwana: Supercontinent Assembly and Breakup* (eds M. Yoshida, B. E. Windley & S. Dasgupta), pp. 57–75. Geological Society of London, Special Publication no. 206.